3. ATMOSPHERE

Alexander Schulz[1], Holger Deckelmann[1], Markus Rex[1,2], Juarez Viegas[9], Matt Boyer[4,9], Zoé Brasseur[5], Matthew Shupe[6,7], Julian Hofer[15], Andreas Raeke[18], Matthew Shupe[6,7], Jackson Osborn[6,7], Michael Lonardi[23], Christian Pilz[15], Byron Blomquist[6,7], Stephen Archer[24], Tuija Jokinen[5], Jonathan Hamilton[7], Radiance Calmer[7]

(not on board) Marion Maturilli[1], Jessie Creamean[8], Heath Powers[3,9], Jim Mather[9,10], David Chu[3,9], Kerri Pratt[11], Gijs de Boer[6,7], Klaus Dethloff[1], Elizabeth Hunke[3], Wieslaw Maslowski[12], Allison McComiskey[4], David Randall[8], Michael Tjernstrom[13], David Turner[7], Johannes Verlinde[14], Ronny Engelmann[15], Hannes Griesche[15], Martin Radenz[15], Dietrich Althausen[1], Holger Baars[1], Patric Seifert[1], Albert Ansmann[15], Andreas Macke[15], Mario Mech[16], Bernhard Pospichal[16], Kerstin Ebell[16], Susanne Crewell[16], Gaël Dubois[17], Luc Blarel[17], Philippe Goloub[17], Ola Persson[6,7], David Costa[6,7], Thomas Ayers[7], Christopher Cox[7], Christopher Fairall[7], Michael Gallagher[6,7], Daniel Gottas[7], Jesse Leach[7], Sara Morris[7], Sergio Pezoa[7], Taneil Uttal[7], Ian Brooks[19], Jennifer Hutchings[20], Don Perovich[21], Timothy Stanton[12], Roberta Pirazzini[22], André Ehrlich[23], Heike Kalesse[1], Andreas Macke[15], Holger Siebert[15], Birgit Wehner[15], Manfred Wendisch[23], Detlev Helmig[6], Chris Fairall[7], Laurens Ganzeveld[25], William Sturges[26], Dean Howard[6], Ludovic Bariteau[6,7], Hélène Angot[6], Hans-Werner Jacobi[27], Kevin Posman[24], Sjoerd Barten[25], Lucy Carpenter[28] Ivo Beck[29], Lauriane Quéléver[5], Tiia Laurila[5], Julia Schmale[29], Mikko Sipilä[5], Tuukka Petäjä[5], Markku Kulmala[5], Gina Jozef[6], John Cassano[6], Dale Lawrence[6], Brian Argrow[6], Steven Borenstein[6], Abhiram Doddi[6], Michael Rhodes[6]

[1]DE.AWI
[2]DE.UNI-Potsdam
[3]GOV.LANL
[4]GOV.BNL
[5]FI.UNI-Helsinki
[6]EDU.CU
[7]GOV.NOAA
[8]EDU.CSU
[9]GOV.ARM
[10]GOV.SANDIA
[11]EDU.UMICH
[12]EDU.NPS
[13]SE.SU
[14]EDU.PSU
[15]DE.TROPOS
[16]DE.UNI-KOELN
[17]FR.UNIV-LILLE
[18]DE.DWD
[19]UK.UNI-LEEDS
[20]EDU.ORSU
[21]EDU.DARTMOUTH
[22]FI.FMI
[23]DE.Uni-Leipzig
[24]ORG.BIGELOW
[25]NL.WUR
[26]UK.AC.UEA
[27]FR.UGA
[28]UK.AC.YORK
[29]CH.EPFL

Grant-No. AWI_PS122_00

A comprehensive summary of the atmospheric measurements during all 5 cruise legs can be found in Shupe et al., 2022.

References

Shupe, MD, Rex, M, Blomquist, B, Persson, POG, Schmale, J, Uttal, T, Althausen, D, Angot, H, Archer, S, Bariteau, L, Beck, I, Bilberry, J, Bucci, S, Buck, C, Boyer, M, Brasseur, Z, Brooks, IM, Calmer, R, Cassano, J, Castro, V, Chu, D, Costa, D, Cox, CJ, Creamean, J, Crewell, S, Dahlke, S, Damm, E, de Boer, G, Deckelmann, H, Dethloff, K, Dütsch, M, Ebell, K, Ehrlich, A, Ellis, J, Engelmann, R, Fong, AA, Frey, MM, Gallagher, MR, Ganzeveld, L, Gradinger, R, Graeser, J, Greenamyer, V, Griesche, H, Griffiths, S, Hamilton, J, Heinemann, G, Helmig, D, Herber, A, Heuzé, C, Hofer, J, Houchens, T, Howard, D, Inoue, J, Jacobi, H-W, Jaiser, R, Jokinen, T, Jourdan, O, Jozef, G, King, W, Kirchgaessner, A, Klingebiel, M, Krassovski, M, Krumpen, T, Lampert, A, Landing, W, Laurila, T, Lawrence, D, Lonardi, M, Loose, B, Lüpkes, C, Maahn, M, Macke, A, Maslowski, W, Marsay, C, Maturilli, M, Mech, M, Morris, S, Moser, M, Nicolaus, M, Ortega, P, Osborn, J, Pätzold, F, Perovich, DK, Petäjä, T, Pilz, C, Pirazzini, R, Posman, K, Powers, H, Pratt, KA, Preußer, A, Quéléver, L, Radenz, M, Rabe, B, Rinke, A, Sachs, T, Schulz, A, Siebert, H, Silva, T, Solomon, A, Sommerfeld, A, Spreen, G, Stephens, M, Stohl, A, Svensson, G, Uin, J, Viegas, J, Voigt, C, von der Gathen, P, Wehner, B, Welker, JM, Wendisch, M, Werner, M, Xie, ZQ, Yue, F. 2022. Overview of the MOSAiC expedition: Atmosphere. Elementa: Science of the Anthropocene 10(1). DOI: https://doi.org/10.1525/elementa.2021.00060

3.1. FROM THE SURFACE TO THE STRATOSPHERE: CHARACTERIZATION OF THE ATMOSPHERIC COLUMN

Alexander Schulz[1], Holger Deckelmann[1], Markus Rex[1,2]

[1]DE.AWI
[2]DE.UNI-Potsdam

(not on board) Marion Maturilli[1]

Objectives

The scientific objectives are summarized in the PS122 Expedition Programme (EXPEDITION PROGRAMME PS122 Polarstern PS122 Tromsø – Bremerhaven 20 September 2019 – 14 October 2020, available via www.awi.de/en/reports) and remained unchanged during Leg 4. Routines and operational procedures developed and done during MOSAiC Leg 1 to Leg 3 had been continued. An overview of the activities and measurements can be found in the former cruise reports. Minor adaptations of scientific priorities and technical realizations based on seasonal changes of the atmospheric physics and additional measurement platforms during Leg 4 had been done**.**

The surface temperatures were mostly around 0°C due to the phase exchange of the surface. Depending on cloud cover and air advection melting was progressively ongoing interrupted by short periods of refreezing of the surface. Cloudy and foggy conditions and calm wind conditions typically below 5m/s wind speed were predominant. No major storm events occurred. The floe was stable during the complete leg and no ridges or leads had been formed. We started to collect data with our equipment on 27 June 2020 with two mobile eddy covariance sledges, followed by the tower measurements (DTS) on 2 July 2020 and finally the tethered balloon operation on 14 July 2020. On 29 July 2020 all instrumentation had been removed from the floe. The ice floe broke into pieces during the 30 July 2020.

The measurement strategies had been slightly adapted to the predominant physics and the infrastructural conditions on the ice floe. This is briefly summarized below.

a) 2, instead of 1, AWI mobile eddy covariance systems (MEC sledges) were installed on the floe to sample more than one footprint area in the same time

b) Lead experiments with both MEC systems had been not conducted due the missing or small temperature difference between open water and the atmosphere during the summer season. The high impact of open leads on the turbulent exchange doesn't exist during summertime. Measurements of heterogeneous footprints (especially roughness) had the priority now.

c) The adapted installation of a fixed 10m tower with a fibre optic cable temperature measurement (Distributed Temperature Sensing measurement) close to Balloon Town during leg 3 was continued and optimized. Furthermore the setup was extended by deploying 60m of fibre optic cable into the upper ocean resulting in a 70m profile connecting the ocean mixed layer with the atmosphere surface layer.

d) DTS experiments on the AWI tethered balloon platform ("Miss Piggy") had been not conducted since the last flight in December 2019 (Leg 2) due to a major damage of some parts of the equipment. This equipment could be repaired at the beginning of Leg 4 resulting in a high demand of conducting these measurements again by chance.

e) The second year ice floe where *Polarstern* moored during Leg 4 (so called "Fortress" part of the floe sampled during the former MOSAiC legs) had only a limited amount of stable and non-flooding areas (mostly ridges) for huge installations like big tents, power hubs etc. Therefore, Balloon Town couldn't be re-established and especially not extended by the second tethered balloon launching site as planned. Additionally, the big TROPOS tether balloon "Beluga" occupied a lot of space for its ground installations and the very limited airspace over the floe. The installation of 2 launching sites with minimum distance of 100m in between couldn't be realized. For that reason, the opportunity to use the Beluga platform for DTS measurements was discussed but the concurrent operation modes (profiling vs. continuous) of both balloon teams had resulted in a major reduction of flight hours for all experiments. We developed a strategy together with the cruise and science leadership for operation of both tethered balloon platforms by adapting the AWI equipment to these new conditions.

f) We decided to modify our AWI tethered balloon ("Miss Piggy") and the repaired DTS measurement equipment* in such a way, so that it can be operated from a Nansen sledge to be flexible concerning the position in case of wind shear and flight operations of Beluga and the helicopter.

   * Silixa XT19076 DTS system stopped to work during Leg 3 (broken fuse) and a mechanical damage of a special solid state calibration unit integrated in cable drum occurred during Leg 2

g) Aerosol sampling, ozone sampling and turbulence sampling payloads flown on the Miss Piggy platform (profiling and continuous measuring mode for aerosol and turbulence probes) in the former legs had been done by instruments attached to the Beluga balloon as partly planned for Leg 4

h) Point d to g resulted in the highest priority for DTS measurements on the modified Miss Piggy platform. Therefore, no other instruments had been flown during Leg 4 on the Miss Piggy platform. Consistent time series of turbulence, aerosol and ozone concentration profiles were covered by instruments flown on the Beluga platform (see Chapter 3.5)

Work at sea

a) On-board Polarstern: Weather Balloons

During the whole leg 4 weather balloons were started from the helicopter deck on-board *Polarstern* an hour before the synoptic times 00UTC, 06UTC, 12UTC and 18UTC. This standard procedure allows that the data at the 100hPa level, at the highest point of the sounding on burst of the balloon (end of ascent), and after the sonde descent can be transmitted near real time to the weather forecast centres via the GTS to be incorporated in the current weather forecast.

Therefore, our measurements improve the forecast of weather at our own position, which is vital in data sparse Polar regions. Additionally, we had two intense observation periods. The first period was from 9 to 10 June 2020 with eight launches daily during travelling through the ice edge region for an enhanced characterization of this transition zone. The second period was from 21 to 22 July 2020 during a 24-hour continuous observation day of the Team ATMO. This means we launched additional radiosondes for the 03 UTC, 09UTC, 15UTC and 21UTC synoptic times.

Due to the stable and calm weather conditions all soundings could be conducted as planned without weather implications. Bathing of the balloons in oil (see leg 3) was not necessary. 98% of the launched balloons reached heights over 30 km, with record heights of 36 km. In total, 269 balloons were launched during Leg 4.

Standard radiosondes were further equipped with add-on sensors on a regular basis (9 sondes in total, cf. Table 3.1.1). We performed ozone soundings on weekly basis and one launch of a CFH (Cryogenic Frost-point Hygrometer) sensor on 10 August 2020. These instruments measure profiles of ozone concentration and stratospheric water vapour, respectively. To carry the additional payload, we use larger 1500 g balloons.

Tab. 3.1.1: Weather balloon ascends with add-on sensors

DShip Device Operation	Synoptic Date	Add-On Sensors
PS122/4_44-57	2020-06-12 18UTC	Ozone
PS122/4_44-100	2020-06-19 12UTC	Ozone
PS122/4_44-152	2020-06-23 18UTC	Ozone
PS122/4_44-229	2020-06-28 12UTC	Ozone
PS122/4_45-128	2020-07-05 12UTC	Ozone
PS122/4_46-145	2020-07-12 12UTC	Ozone
PS122/4_47-116	2020-07-19 12UTC	Ozone
PS122/4_48-164	2020-07-26 18UTC	Ozone
PS122/4_50-5	2020-08-03 12UTC	Ozone
PS122/4_50-70	2020-08-10 18 UTC	Ozone+CFH

b) On the ice: Tethered Balloon

Due to the limited air space for flight operations and ground space for installations on the ice floe, we had to minimize the measurement setup of Miss Piggy. There was no space for several tents, especially not for a big hangar tent used during the prior legs. We equipped a Nansen sledge with all necessary tethered balloon equipment (fibre optic cable drum, tether sonde ground station, DTS System, winch). Miss Piggy had to be parked at about 8m height in the field. Deflation of the balloon was planned for storm events but had been never done due to the calm wind conditions during Leg 4. First of all we needed to conduct a proof of concept flight with the rearranged setup. This was done on 14 July under coordination with the Beluga and helicopter team. The test flight was successful and the setup could be used for further flights. All following flights had been scientifically coordinated within the ATMO team, especially the Beluga team, resulting in several ours of co-deployments of Beluga and

Miss Piggy. The short ground distance between both balloons (about 60m) allows the synthesis of the measurements from both platforms. In total 5 different Miss Piggy setups (different DTS profiling altitudes) had been conducted which are listed below.

Tab. 3.1.2: Measurement times on the Miss Piggy platform (based on DTS instrument time stamps)

PS122_4_47_193_XT19077_250m_MsPiggy_20200714_20200714
14.07.2020 12:44:16 UTC - 14.07.2020 14:42:00 UTC
PS122_4_47_194_XT19077_250m_MsPiggy_20200715_20200715
15.07.2020 09:29:41 UTC - 15.07.2020 11:27:22 UTC
PS122_4_47_195_XT19077_515m_MsPiggy_20200715_20200720
15.07.2020 13:09:34 UTC - 16.07.2020 00:00:00 UTC (~11h data)
16.07.2020 00:00:00 UTC - 16.07.2020 09:11:01 UTC (~09h data)
16.07.2020 11:15:27 UTC - 16.07.2020 13:00:00 UTC (~02h data)
16.07.2020 13:00:00 UTC - 16.07.2020 14:41 UTC (maintenance)
16.07.2020 14:41:00 UTC - 17.07.2020 00:00:00 UTC (~09h data)
17.07.2020 00:00:00 UTC - 17.07.2020 02:10:01 UTC (~02h data)
17.07.2020 06:52:57 UTC - 17.07.2020 13:07:23 UTC (~06h data)
19.07.2020 12:24:30 UTC - 20.07.2020 00:00:00 UTC (~10h data, 1h maintenance)
20.07.2020 00:00:00 UTC - 20.07.2020 12:32:02 UTC (~07h data, from 07:00 UTC maintenance)
PS122_4_48_225_XT19077_300m_MsPiggy_20200721_20200721
21.07.2020 08:36:16 UTC - 21.07.2020 13:23:42 UTC (~5h data)
PS122_4_48_226_XT19077_575m_MsPiggy_20200722_20200722
22.07.2020 05:19:25 UTC - 22.07.2020 07:48:40 UTC (~1h data, from 06:30 UTC maintenance)
PS122_4_48_227_XT19077_165m_MsPiggy_20200725_20200720
25.07.2020 08:39:20 UTC - 26.07.2020 00:00:00 UTC (~14h data, 1h maintenance)
26.07.2020 00:00:00 UTC - 26.07.2020 11:54:26 UTC (~12h data)
26.07.2020 13:01:08 UTC - 27.07.2020 00:00:00 UTC (~11h data)
27.07.2020 00:00:00 UTC - 27.07.2020 13:42:09 UTC (~14h data)
27.07.2020 14:57:19 UTC - 28.07.2020 00:00:00 UTC (~09h data)
28.07.2020 00:00:00 UTC - 28.07.2020 12:10:09 UTC (~12h data)

Within the setup **PS122_4_47_195_XT19077_515m_MsPiggy_20200715_20200720** and **PS122_4_48_227_XT19077_165m_MsPiggy_20200725_20200720** in total 6 over night flights had been conducted to sample the diurnal cycle of the atmospheric surface layer and full atmospheric boundary layer, respectively. In total about 137 measurement hours had been realized. We used the Silixa XT19077 DTS system. The calibration sections had been realized with the repaired solid phase calibration bathes (SOPHABs) which had been removed from the broken SOPHAB fibre drum. The fibre was routed twice (after the pigtail and before the atmospheric profile) through these calibration sections to realize each section (warm and cold) two times along the fibre for each line of the helical AFL optical fibre. All DTS setups listed above had been configured with a temporal sampling step of 5s resulting in about 100000 temperature profiles. On 21 July 2020 UAV operations (see Chapter 3.8) moved from the FYI part of the floe to the Met City SYI area, about 150m away from the Met City tower. Purpose of this was to realize the co-deployment of all flying platforms over SYI allowing the synthesis of the different measurements. In the following days Beluga (several payloads), Miss Piggy (DTS profiling) and UAV (several payloads) were operated in

overlapping time periods and covered overlapping footprints. This resulted in a unique time series with measurements coinciding in time and space.

Three minor issues occurred during the flight operations during Leg 4. During the overnight flight from 19 to 20 July 2020 the tether rope and fibre optic cable iced strongly resulting in a descending of the balloon due to the additional payload. Both lines had a lot of slack hanging nearly parallel to the ground from the sledge to the ship (about 200m) due to the wind drift of the balloon and laid on a boom of the *Polarstern* chimney since 20 July about 01:48 UTC. This could be solved by lifting both lines above the chimney boom. Unfortunately the optical fibre broke at about 300m of the 515m profile. The last 200m of the profile had been cut resulting in the 300m configuration flown within the setup **PS122_4_48_225_XT19077_300m_MsPiggy_20200721_20200721**.

During the ascend of the 300m profile on 21 July 2020 a small sling within the fibre resulted in a break of one of the helical lines of the AFL optical fibre cable at about 250m. Therefore this profile was only sampled with one helical line. We prepared a new 2000m fibre cable drum on 21 July 2020 afternoon used for all following experiments.

On 22 July 2020 the tether line of the Beluga balloon entangled to the Miss Piggy tether rope at 06:30 UTC by a fast wind direction shear during the co-deployment **PS122_4_48_226_XT19077_575m_MsPiggy_20200722_20200722**. This resulted in unrepairable damage of Miss Piggy balloon no. 5 used for all Leg 4 flights so far. After 25 July 2020 a spare balloon was used. The tethersonde anemometer (SN A2637144) used for all prior flights was also damaged and was replaced by another tethersonde (SN F0539540). On 26 July 12:20 UTC this sonde stopped sending data and was replaced by yet another tethersonde (SN C1629526), which was used until the end of Leg 4. Details of the measurements had been saved in field books (contact: Alexander Schulz, AWI).

c) On the ice: Mobile Eddy Covariance System

Our floe had a first year ice (FYI) and second year ice (SYI) part. The surface of both parts of the floe was a mixture of old ridges, melting snow patches and growing melt ponds. The SYI surface had a heterogeneous albedo distribution due to sediments, particles and bioactivity. The FYI was less contaminated by sediments and showed a fast change of the surface structure during the melting process (fast growing melt ponds). Ridges influenced strongly the ice surface roughness which implied the hypothesis that the surface drag was increased resulting in an increased momentum flux in these areas. The different albedo influenced the surface radiation balance. To cover all aspects of the system we coordinated our mobile eddy covariance system deployment with an ASFS deployment (PI: Matthew Shupe, see Chapter 3.4). The ASFS was fully equipped to cover all terms of the surface energy budget equation. Therefore it was deployed to the FYI area. The Met City tower (contact: Matthew Shupe, see Chapter 3.4), also covered all budget terms, needed a stable underground and was installed on a big ridge in the SYI area. Depending on the wind direction the Met City tower could not sample optimally all footprint areas around. Therefore we decided (Matthew Shupe, Alexander Schulz) to move and arrange the AWI MEC systems in such a way, that the missing or disturbed areas were covered by the AWI MECs. The resulting measurement periods are listed below. The exact GPS positions of the sledges are recorded by the MEC systems and had been additionally measured manually for independent heading calculation of the systems. Details of the measurements had been saved in field books (contact: Alexander Schulz, AWI).

Tab. 3.1.3: List of the mobile eddy covariance measurement

MEC 1 Met City (about 20m away from Met City tower, “left” of the big ridge)
27.06.2020 12:34 UTC – 28.07.2020 13:30 UTC (25 hours)
28.06.2020 13:52 UTC – 01.07.2020 07:43 UTC (65.5 hours)

01.07.2020 08:20 UTC – 03.07.2020 12:00 UTC (52 hours)
03.07.2020 12:36 UTC – 06.07.2020 12:25 UTC (71.5 hours)

MEC 1 50m away from Balloon Town, “right” of the big ridge
11.07.2020 14:16 UTC - 15.07.2020 19:30 UTC (101.5 hours)
19.07.2020 15:10 UTC - 23.07.2020 11:49 UTC (92.5 hours)
23.07.2020 12:05 UTC - 28.07.2020 07:00 UTC (115 hours)
28.07.2020 08:44 UTC - 29.07.2020 12:30 UTC (27.5 hours)

MEC 2 Met City (about 50m away from Met City tower, “right” of the big ridge)
27.06.2020 13:23 UTC - 28.06.2020 14:25 UTC (25 hours)
28.06.2020 14:30 UTC - 01.07.2020 08:31 UTC (66 hours)
01.07.2020 08:45 UTC - 03.07.2020 09:31 UTC (48.5 hours)

MEC 2 between Ocean City and Balloon Town
06.07.2020 12:54 UTC - 08.07.2020 15:18 UTC (50 hours)
08.07.2020 15:23 UTC - 09.07.2020 08:06 UTC (16.5 hours)
09.07.2020 08:18 UTC - 10.07.2020 14:33 UTC (30 hours)

MEC 2 50m away from Balloon Town, “right” of the big ridge, MEC 1 comparison
10.07.2020 15:18 UTC - 16.07.2020 17:00 UTC (145.5 hours)

In total we collected about 550 hours with the MEC 1 system and 381 hours with MEC 2 system of atmospheric turbulence data from various footprint areas during Leg 4.

d) On the ice: 10m + 60m Atmosphere Ocean profile tower

One of the most crucial parts of atmospheric boundary layer are the first meters above the ground. During Leg 3 one mobile 10m tower was installed close to Balloon Town and was equipped with fibre optic cable (DTS measurement). For continuation of these high resolution temperature profiling we reinstalled the 10m about 30m “behind” the ADCP hole of Ocean City, named Fiber Town in the following. The tower was installed in a flat area of the SYI part of the floe about 100m away from the Met City tower. Additionally, we put 60m of fiber cable into the ocean to sample continuously temperature variations of the upper ocean mixed layer at the same spot. This installation was coordinated within the ATMO and OCEAN team to achieve an optimal sampling network and avoidance of inference with other ocean sensor deployments. Furthermore, the 70m Fiber Town profile complemented the temperature measurements from the Met City tower with continues temperature measurements in the first meters over flat ice (Met City tower was installed on a ridge). The 60m continuous ocean temperature profiling of the ocean mixed layer complemented the discrete MSS and CTD profiles.

The setup of the Leg 4 Fiber Town setup was updated compared to the installation during leg 3. First, the helical optical fibre cable was routed twice through the full 70m profile, resulting in 4 measurements at each point in space. Second, two solid state calibration sections (SOPHABs) had been installed to realize an optimal setup for temperature calibration in the post processing. We used the Silixa XT19076 system for this setup. We used 10s sampling time step for this setup.

Tab. 3.1.4: Measurement time of the combined 10m atmosphere and 60m ocean DTS profile

70m Fiber Town DTS temperature profile
02.07.2020 12:44 UTC - 29.07.2020 08:26 UTC (582 hours)
11.07.2020 22:11 UTC - 12.07.2020 18:51 UTC break due to disconnection of power
17.07.2020 12:01 UTC - 18.07.2020 12:03 UTC break for data collection

In total we collected 582 hours of data resulting in 200070 high resolution temperature profiles (time steps). Details of the measurements had been saved in field books (contact: Alexander Schulz, AWI).

A fully georeferenced floe map assembled from the ALS scans (Laser scans of the floe, contact: Gerit Birnbaum) with all measurement sites marked will be published in future. Personal contacts for interim floe map products are Gerit Birnbaum (AWI) or Stefan Hendricks (AWI).

Preliminary (expected) results

Expected results from the planning phase are summarized in the PS122 Expedition Programme (EXPEDITION PROGRAMME PS122 Polarstern PS122 Tromsø – Bremerhaven 20 September 2019 – 14 October 2020, available via www.awi.de/en/reports).

Turbulence measurements from both MEC systems could fill some sampling gaps of the MetCity tower and provide data from footprints not optimally covered by any other instrument on the SYI part of the floe. Therefore sparely available flux data was collected.

The 70m profile realized the interconnection between the atmosphere and the ocean boundary layer with a homogenous measurement. Together with flux measurements within the atmospheres' and oceans' flux measurements (eddy covariance measurements and microstructure profiling) an optimized synthesis of the measurements concerning the intersystem exchange can be realized. The 10m atmosphere profile complements the missing first meters of the Met City tower measurements and gives an optimal overlap to the flat SYI area of the floe. An example of a 24h time period is given in the following Figure 3.1.1.

The upper part of the profile time series shows the atmosphere temperature fluctuations during the day. The bottom 60m parts shows the nearly isothermal ocean temperature. In between the 0°C temperature locked sea water in the ice hole (ice thickness about 1.5m) is visible.

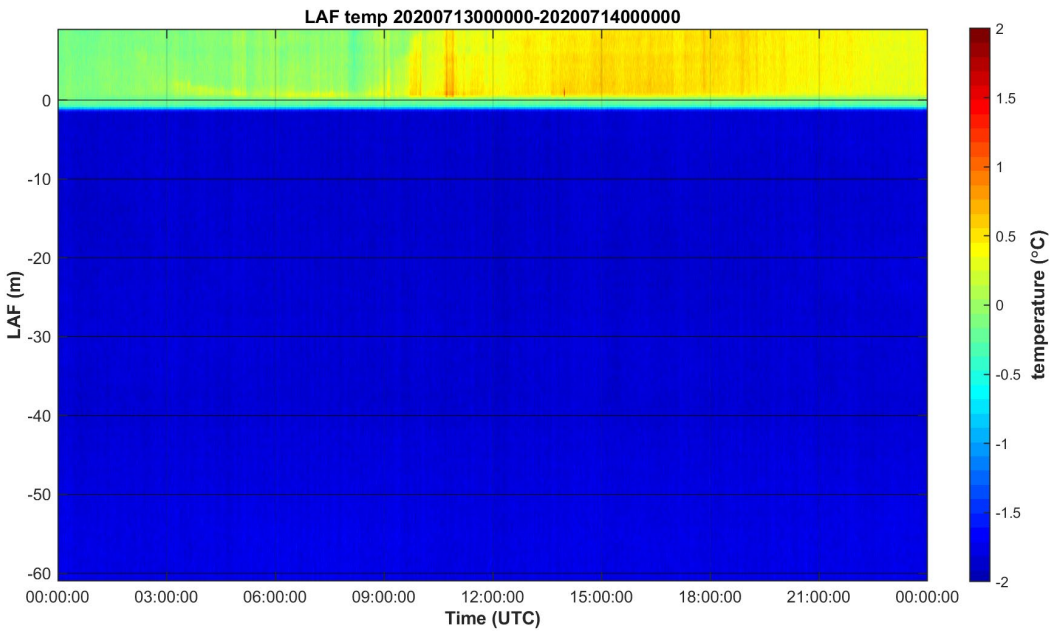

Fig. 3.1.1: time series of the 10m atmosphere + 60m ocean profile between 13th – 14th July 2020; temporal resolution 10s, spatial sampling 25cm (60cm physical resolution)

Additionally to the expected results mentioned in the PS122 expedition programme the tethered balloon based temperature profile measurements had been carefully coordinated with other measurements on the other airborne platforms during Leg 4. Therefore these profiles are supposed to realize and optimize the synthesis of the multidisciplinary measurements. Horizontal transect flights from UAV based instruments can be connected to distinct vertical profiles of aerosol and turbulence via the high resolution temperature profile time series.

Data management

All data are handled, documented, archived and published following the MOSAiC data policy (see APPENDIX).

All radiosonde data have been transmitted to the GTS in near real-time to assure their availability for numerical weather forecast. All sounding data (radiosonde, ozone sonde, CFH, COBALD) and according auxiliary measurements are stored in the MCS. Upon the end of Leg 4, the preliminary sounding data will be processed at the GRUAN Lead Centre in Lindenberg, Germany. The final sounding data will be stored at the PANGAEA data repository (World Data Center PANGAEA Data Publisher for Earth & Environmental Science; http://www.pangaea.de/)) and handled, documented, archived and published following the MOSAiC data policy.

The DTS light backscatter profiles (incl. preliminary temperature profiles) were also stored in the MCS at the end of Leg 4. The final data processing of the DTS temperature profiles will be conducted at the Alfred Wegener Institute in Potsdam, Germany (contact: Alexander Schulz, alexander.schulz@awi.de). Final data products will be stored at the PANGAEA data repository (World Data Center PANGAEA Data Publisher for Earth & Environmental Science; http://www.pangaea.de/)) and handled, documented, archived and published following the MOSAiC data policy.

The eddy covariance data (incl. preliminary result of field processing) were stored in the MCS at the end of Leg 4. The final data processing of the DTS turbulence data will be conducted at the Alfred Wegener Institute in Potsdam, Germany (contact: Alexander Schulz, alexander.schulz@awi.de). Final data products will be stored at the PANGAEA data repository (World Data Center PANGAEA Data Publisher for Earth & Environmental Science; http://www.pangaea.de/)) and handled, documented, archived and published following the MOSAiC data policy.

3.2 DOE ATMOSPHERIC RADIATION MEASUREMENT PROGRAM'S MOBILE FACILITY

Juarez Viegas[4], Matt Boyer[4], Zoé Brasseur[13], Matthew Shupe[1,2]

(not on board:) Jessie Creamean[6], Heath Powers[3,4], Jim Mather[3,5], David Chu[3,4], Kerri Pratt[7], Gijs de Boer[1,2], Klaus Dethloff[8], Elizabeth Hunke[4], Wieslaw Maslowski[9], Allison McComiskey[10], David Randall[6], Michael Tjernstrom[11], David Turner[2], Johannes Verlinde[12]

[1]EDU.CU
[2]GOV.NOAA
[3]GOV.ARM
[4]GOV.LANL
[5]GOV.SANDIA
[6]EDU.CSU
[7]EDU.UMICH
[8]DE.AWI
[9]EDU.NPS
[10]GOV.BNL
[11]SE.SU
[12]EDU.PSU
[13]FI.UNI-Helsinki

Objectives

To understand the changing Arctic sea ice at a fundamental level requires a detailed accounting of energy flow through the sea ice system. While it is clear that atmospheric energy fluxes are critically important for the sea ice energy budget, many processes controlling these fluxes, and their interactions, are poorly understood and represented in numerical models. This project aims to observe specific processes that control the flow of energy through the Arctic atmospheric system and thereby to address pressing science questions under four broad topics.

(a) Surface Energy Budget: What is the annual evolution of the surface energy budget over young sea ice? What are the key process interactions determining the surface energy budget and specifically variability in surface radiation?

(b) Clouds and Precipitation: What factors determine Arctic cloud phase partitioning? What role do clouds and precipitation play in determining low-level atmospheric structure? How does surface inhomogeneity influence the spatial structure of cloud-precipitation systems?

(c) Aerosols: How do aerosol physical, chemical, and optical properties over sea ice vary seasonally? What sources and transport patterns are responsible for variability in Arctic aerosol? What are the radiative and cloud-nucleating properties of Arctic aerosol?

(d) Boundary Layer Structure: What are the properties and effects of stably stratified turbulence in the Arctic boundary layer? What are the effects of a thinned ice cover on boundary layer stability and heat fluxes? How do surface- and cloud-driven dynamics impact the boundary layer structure?

Work at sea

To provide the diverse and detailed atmospheric measurements needed to address the primary scientific objectives of the project, the US Department of Energy's Atmospheric Radiation Measurement (ARM) Program (www.arm.gov) has deployed its second ARM Mobile Facility (AMF-2) onboard and nearby *Polarstern* during MOSAiC. This extensive suite of instruments is operated in a collection of six laboratory sea-containers installed on the bow of *Polarstern*, one laboratory container installed on the *Polarstern* P-deck, as well as various instruments installed at Met City out on the sea ice of the Central Observatory. ARM has also provided funding support for one half of the meteorological radiosonde program led by AWI during MOSAiC, as well as personnel support for launching some of these soundings. The

AMF-2 facility can be described via five instrument collections, which are captured in Table 3.2.1.

Tab. 3.2.1. All instruments installed and operated by the DOE ARM program, including the measurement objectives, installation location, and start date for observations.

Instrument	Measurement Objectives	Installation Location	Start of Observations
Meteorology and Winds			
Radiosonde Program (support for ½ of equipment)	Profiles of temperature and humidity	Helideck	20 Sept
Present Weather Detector (PWD)	Visibility	(1) P-deck port side; (2) Met City	17 Oct
Beam-steerable radar wind profiler (BSRWP)	Wind profiles	KAZR lab (C3)	5 Oct
Doppler lidar (DL)	Wind profiles, turbulence	Top OPS lab (C4)	7 Oct
Cloud Properties and Processes			
2-channel microwave radiometer (MWR2C)	Liquid water path and precipitable water vapor	Lower P-deck port side	16 Oct
3-channel microwave radiometer (MWR3C)	Liquid water path and precipitable water vapor	Lower P-deck port side	8 Oct
Ka-Band ARM Zenith Radar (KAZR)	Cloud occurrence and properties	KAZR lab (C3)	5 Oct
Marine W-Band ARM Cloud Radar (MWACR)	Cloud occurrence and properties	Top of OPS lab (C4)	16 Oct
High Spectral Resolution Lidar (HSRL)	Cloud & aerosol properties	OPS lab (C4)	10 Oct
Micropulse Lidar (MPL)	Cloud & aerosol properties	OPS lab (C4)	5 Oct
Ceilometer (CEIL)	Cloud base height	Lower P-deck port side	8 Oct
Total Sky Imager (TSI)	Hemispheric sky views	P-deck	23 Mar
Precipitation			
Ka-Band Scanning ARM Cloud Radar (Ka-SACR)	Cloud and precipitation spatial distribution	P-deck, starboard side	5 Oct
Parsivel2 Laser Disdrometer (LDIS)	Fall velocity and precipitation rate of precipitation	(1)P-deck port side; (2)Met City double Altar shield	(1) 30 Oct, (2) 14 Nov
Pluvio2 Weighing Bucket Rain Gauge (WBRG)	Precipitation mass	Met City in double Altar shield	30 Oct
Siphon Rain Gauge (SRG)	Precipitation mass	P-deck port side	30 Oct
Radiation			
Marine Atmospheric Emitted Radiance	Spectral infrared radiation, both downwelling and	Lower P-deck port side, view to	9 Oct

Interferometer (MAERI)	upwelling	port side ice	
Cimel Sunphotometer (CSPHOT)	Atmospheric transmission & scattering during daylight	P-deck	18 June
Fast Rotating Shadowband Radiometer (FRSR)	Direct and diffuse components of downward solar flux	P-deck	14 Oct
Ground Radiometer System (GNDRAD) – PIR, PSP	Upwelling shortwave and longwave radiation	Met City "swingset"	14 Oct
Ground Infrared Thermometer (IRT)	Ground temperature with wide field-of-view	Met City "swingset"	30 Oct
Multifilter Radiometer 3-meter (MRF3M)	Reflected radiative flux in narrow bands	Met City "swingset"	14 Oct
Ice Radiometer System (ICERAD) – PIR, PSP, SPN1	Downwelling shortwave and longwave radiation, with shortwave direct and diffuse	Met City	14 Oct
Shipboard Radiometer System (SHIPRAD) – PIR, PSP, SPN1	Downwelling shortwave and longwave radiation, with shortwave direct and diffuse	(1) P-deck port side; (2) P-deck starboard side	(1) 7 Oct; (2) 7 Oct
Sky Infrared Thermometer (IRT)	Sky temperature with narrow field-of-view	Met City "swingset"	14 Oct
Aerosols and Gases			
Automated Weather Station (AOSMET)	Pressure, temperature, relative humidity, winds	AOS inlet on AOS lab (C5)	9 Oct
Trace Gas Monitors	Concentrations: carbon monoxide, nitrous oxide, water vapor	AOS lab (C5)	9 Oct
Ozone Monitor	Concentration of ozone	AOS lab (C5)	9 Oct
Aerosol Chemical Speciation Monitor (ACSM)	Bulk chemical composition	AOS lab (C5)	8 Nov
Condensation Particle Counter (CPC)	Total particle concentration for sizes >10nm	AOS lab (C5)	8 Oct
Ultrafine Condensation Particle Counter (UCPC)	Total particle concentration for sizes >3nm	AOS lab (C5)	8 Oct
Cloud Condensation Nuclei Counter (CCN)	Concentration of cloud condensation nuclei	AOS lab (C5)	8 Nov
Scanning Mobility Particle Sizer (SMPS)	Aerosol size distribution	AOS lab (C5)	9 Oct
Ultra-High Sensitivity Aerosol Spectrometer (UHSAS)	Aerosol size distribution	AOS lab (C5)	7 Oct
Humidified Tandem Differential Mobility Analyzer (HTDMA)	Aerosol size distribution exposed to different moisture levels	AOS lab (C5)	28 Sept

Single Particle Soot Photometer (SP2)	Soot mass of aerosol particles	AOS lab (C5)	15 Oct
Particle Soot Absorption Photometer (PSAP)	Bulk aerosol absorption	AOS lab (C5)	8 Oct
Nephelometer (NEPH)	Total aerosol scattering at 450, 550, and 700 nm wavelengths	AOS lab (C5)	8 Oct

In addition to the core AMF-2 instruments, ARM has agreed via a proposal process to host and operate instrumentation for two collaborating scientists, Drs. Jessie Creamean and Kerri Pratt. These guest instruments complement the core ARM measurements by the addition of ice nucleus filters, drum samplers, and impactors, all sampling off of the Aerosol Observing System's inlet.

The ARM facility was supported on MOSAiC Leg 4 by 3 on-site technicians (Viegas, Boyer and Brasseur). Operations during Leg 4 were generally robust, with the following issues.

- The X-band Scanning ARM Cloud Radar (X-SACR) system never operated robustly in spite of many attempts to replace, fix, or modify different components; thus, the only scanning radar system available is the Ka-band component of the SACR.
- The AOS system samples air through an inlet and has a special design to minimize sampling of ship's exhaust; this includes monitoring parameters like carbon monoxide to trigger a back flow through the stack during periods of pollution. Thus, for certain periods, typically determined by wind direction, aerosol sampling was not possible.
- The 3-channel microwave radiometer (MWR3C) had a problem with the elevation motor for most of Leg 3. The elevation motor failed permanently and the MWR3C was taken out of service in late April.
- Due to software issues the Fast Rotating Shadow band Radiometer (FRSR) was not operational for the entire Leg 4.
- The Humidified Tandem Differential Mobility Analyzer (HTDMA) had a problem with the drain system during Leg 2. Spares were sent for Leg 4; the water pump was replaced and one of the instrument's valve was inspected and fixed. Mid-June the instrument was finally operating properly and remained operational for the rest of Leg 4.
- The Cimel sun photometer (CSPHOT) was installed on 18 June 2020 on the P-deck.
- The Single Particle Soot Photometer (SP2) was installed in the AOS on 19 June and was removed again on 31 July due to ship movement upon leaving the MOSAiC ice floe. The instrument will be reinstalled when the ship is stationary again in Leg 5.
- The Siphon Rain Gauge (SRG) was taken out of service on the 18th of June due to communication issues with the data logger. The instrument communication cables were heavily corroded and the issue is not serviceable onsite.
- The Aerosol Chemical Speciation Monitor (ACSM) was down on 23 June due to a power issue. After troubleshooting for several days the problem was identified and one of the power supply of the ACSM was replaced with an external component. The instrument was restarted on 8 July and was running normally for the rest of the Leg 4.
- The Sea State Camera, which is used for the purposes of data validation for the MAERI was taken out of service near the end of April due to a part failure. A replacement part was sent for Leg 4 and the camera was reinstalled on 8 June.

- During Leg 3, ARM instrumentation at Met City was taken down and packed away. The Met City instrument set was reinstalled during Leg 4 on 26 June and 3 July 2020. Data was collected manually on a regular basis for the entire Leg 4. The instruments were taken down and packed away at the end of the ice floe life, between 27 and 29 July 2020.
- Due to the departure of the Polarstern from the ice floe, the ARM data system was partially shut down for the voyage on 31 July. The data system will resume operation during Leg 5 once a new drift position has been established. As a result of the data system shutdown, only a partial set of instruments will be run during the transit period. Instruments left running on the ship during the transit period continue to record data independently of the data system.
- Other short-term issues with ARM instrumentation include temporary interruptions to operations of the MWR2C, MAERI, BSRWP, CO_N2O, MWACR, KAZR, ACSM, HSRL. Otherwise, all systems operated rather robustly for the duration of Leg 4.

Preliminary (expected) results

Primary results from the AMF-2 deployment at MOSAiC will be an extensive collection of high-quality data sets from the AMF-2 instrumentation that are as continuous as possible for the full year. These data sets will be quality assured by a large team of instrument mentors and facility managers that will not participate in the field at MOSAiC. Based on these data sets, a suite of value-added products will also be derived to provide information on geophysical parameters related to the atmospheric state, clouds, aerosols, vertical atmospheric structure, and others. These data sets are intended to support a great deal of process-based research in support of advancing knowledge, assessing models, and developing improved models for representing climate processes.

Data management

All data produced by the ARM Program during MOSAiC Leg 4 has been automatically ingested and stored on ARM's onboard "site data system," which performs many operational tasks involved with data management, initial data ingesting and formatting, data quality checks, and the production of quicklook plots of the data. Quicklooks are available via a web page to other scientists onboard *Polarstern* (https://192.168.3.33:8443) and to the general public (https://dq-amfc2.amf.arm.gov). With nearly 36 TB of data produced during Leg 4, it has been agreed that this data will not initially be uploaded to the MOSAiC Central Server, however, MOSAiC scientists can get access to the raw data through a free account on ARM's site data system (192.168.3.33:22) by obtaining credentials from the ARM data manager (see ARM technicians onsite). After MOSAiC Leg 1, and all subsequent legs, the full set of collected data are physically transported to the ARM data management facility and promptly ingested into a full set of processed data files that will then be publicly available via the ARM Data Archive (www.archive.arm.gov). Raw data will be available within a couple of weeks of its arrival at the data management facility. Based on this raw data, a suite of value-added products will also be developed in the following months, with these products also being served at the ARM Archive. Appropriate meta-data sharing and cross-linking will occur via the MOSAiC Central Storage and with PANGAEA (World Data Center PANGAEA Data Publisher for Earth & Environmental Science (www.pangaea.de)) according to the protocol agreed upon between these two archives.

References

None

3.3 TROPOS – OCEANET: REMOTE SENSING OF THE ANNUAL CYCLE OF AEROSOL, CLOUD, AND CORRESPONDING RADIATION CLOSURE STUDIES IN THE CENTRAL ARCTIC

Julian Hofer[1], Andreas Raeke[4]

(not on board:) Ronny Engelmann[1], Hannes Griesche[1], Martin Radenz[1], Dietrich Althausen[1], Holger Baars[1], Patric Seifert[1], Albert Ansmann[1], Andreas Macke[1], Mario Mech[2], Bernhard Pospichal[2], Kerstin Ebell[2], Susanne Crewell[2], Gaël Dubois[3], Luc Blarel[3], Philippe Goloub[3]

[1]DE.TROPOS
[2]DE.UNI-KOELN
[3]FR.UNIV-LILLE
[4]DE.DWD

Objectives

Measurements of the atmospheric state in the Arctic are extremely rare and of great interest for climate research in this unique and changing environment. The mobile facility OCEANET is an ongoing observational initiative of TROPOS for aerosol and cloud profiling as well as radiation budget measurements in maritime environments onboard research vessels since 2007 (Kanitz et al., 2013, Bohlmann et al., 2018). One of the key foci for TROPOS lies on heterogeneous ice formation processes in different areas of the world (e.g., Kanitz et al, 2011) and their radiative impact. During MOSAiC PS122/4 the OCEANET state-of-the-art en-route measurements were implemented on *Polarstern* in order to establish a full Arctic annual aerosol, cloud, and radiation data record.

The following research question are addressed within this project:

- How do aerosol- and cloud properties influence the annual cycle of short-wave and long-wave radiation under different meteorological conditions in the Arctic?
- How often does ice formation in warm (T > –10 °C) stratus clouds occur and what are possible freezing mechanisms under clean Arctic conditions?
- Can we observe different ice-formation rates in the presence of local and long-range transported ice nucleating particles?
- Will Arctic clouds increase or suppress the currently observed Arctic warming?

An additional focus is on ESA's Aeolus wind mission. OCEANET data will also support the CAL/VAL activities of this lidar satellite within the EVAA project.

Work at sea

The OCEANET container of TROPOS was already installed on the bow of *Polarstern* at the container location C8 during MOSAiC Leg 1 (see Fig. 1).

Since then continuous measurements with the

- the multi-wavelength Raman depolarization lidar Polly^{XT} (Engelmann et al., 2016),
- the microwave radiometers HATPRO (TROPOS) and LHUMPRO (UCologne),
- the ULille CIMEL sun/sky/lunar photometer (Yin et al., 2019),
- two disdrometers: OTT Parsivel-2 and 2DVD,
- a total-sky imager,
- a pyranometer and a pyrgeometer,
- a basic DWD weather station (T,p,r.h.)

were performed. Additionally, for Leg 4, a handheld Microtops -2 sun photometer was brought to *Polarstern*.

A solar- and near-infrared irradiance spectrometer (CORAS/SRAPP) was added during Leg 3 with the return of daylight. During Leg 4, CORAS measured almost continuously and was regularly calibrated with a calibration lamp.

Fig. 1: Location of the Oceanet container at the bow of Polarstern (left). Location of the Parsivel-2 and pyranometer and pyrgeometer on the bow crane (right).

All instruments had to be monitored for proper operation and several maintenance and calibration tasks were performed to ensure high data quality. The microwave radiometers operated continuously, except during calibration. HATPRO and LHUMPRO were calibrated with liquid nitrogen back at the floe on 6 July. The lidar Polly^{XT} also operated continuously. Gaps were only caused by maintenance work on the container roof as well as crane and helicopter operations above the OCEANET container.

The CIMEL sun photometer became permanently broken at the beginning of Leg 4. Instead, the Microtops-2 sun photometer could be operated at 15 days during clear sky conditions.

A replacement Parsivel-2 laser disdrometer was installed on the bow crane on 19 June. It measured 8 days in parallel to the ARM Parsivel-2, which was installed on the OCEANET container during Leg 3. On 27 June, the ARM Parsivel-2 was then dismounted from OCEANET and deployed on the ice.

The 2DVD operated continuously, apart from minor maintenance tasks.

The pyranometer and pyrgeometer continued to measure on the bow crane. This location is less affected by shading from the ships superstructure than the container roof. The installation of the Parsivel-2 laser disdrometer on the bow crane might cause some shading.

In addition to the technical setup and maintenance of the OCEANET instrumentation, an automatic profile retrieval algorithm for Polly^{XT} (dubbed Picasso) was used to make profiles of optical properties available in near real-time. This automatic dataset will be reanalyzed later according to PollyNET standards (Baars et al., 2016).

One of the main goals of this project is to link the aerosol information to cloud structure and radiative effects. For this purpose, we could make use of the preliminary data from the ARM KAZR cloud radar (Chapter 3.2), the regular radiosoundings on board (Chapter 3.1), and from the OCEANET lidar and microwave radiometer data and implement the Cloudnet algorithms (Illingworth et al., 2007). In this way, synergistic products, like classification masks

and microphysical retrievals, could already be derived shortly after the measurements. All quicklooks were made available within *Polarstern's* internal network.

Preliminary (expected) results

Direct sun measurements of aerosol optical thicknesses (AOT) during Leg 4 were only possible with the handheld Microtops 2 sun photometer. During a few days, full daily coverage of AOT measurements were possible (e.g., Fig. 2). A comparison to the ARM CIMEL sun photometer operated in vertical pointing "ship mode" could be of benefit.

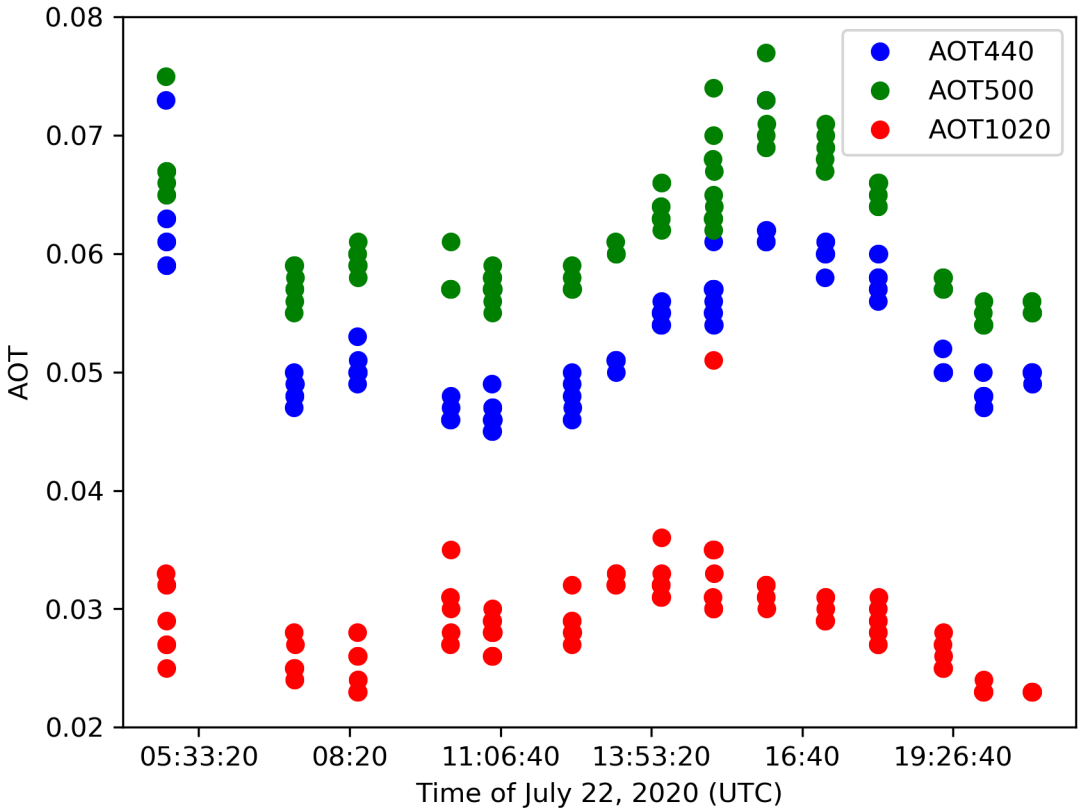

Fig. 2: Aerosol optical thickness at 440 nm (blue), 500 nm (green), and 1020 nm wavelength (red) measured by Microtops 2 handheld sun photometer on 22 July.

A comparison of the two Parsivel-2 laser disdrometers on the container roof and the bow crane can be done during the 8 overlapping days. The day with most precipitation during this period was 26 June, where the two disdrometers provide similar results (Fig. 3). The disdrometer measurements (2DVD and Parsivel-2) need still to be compared to other disdrometers on the ship and the ice.

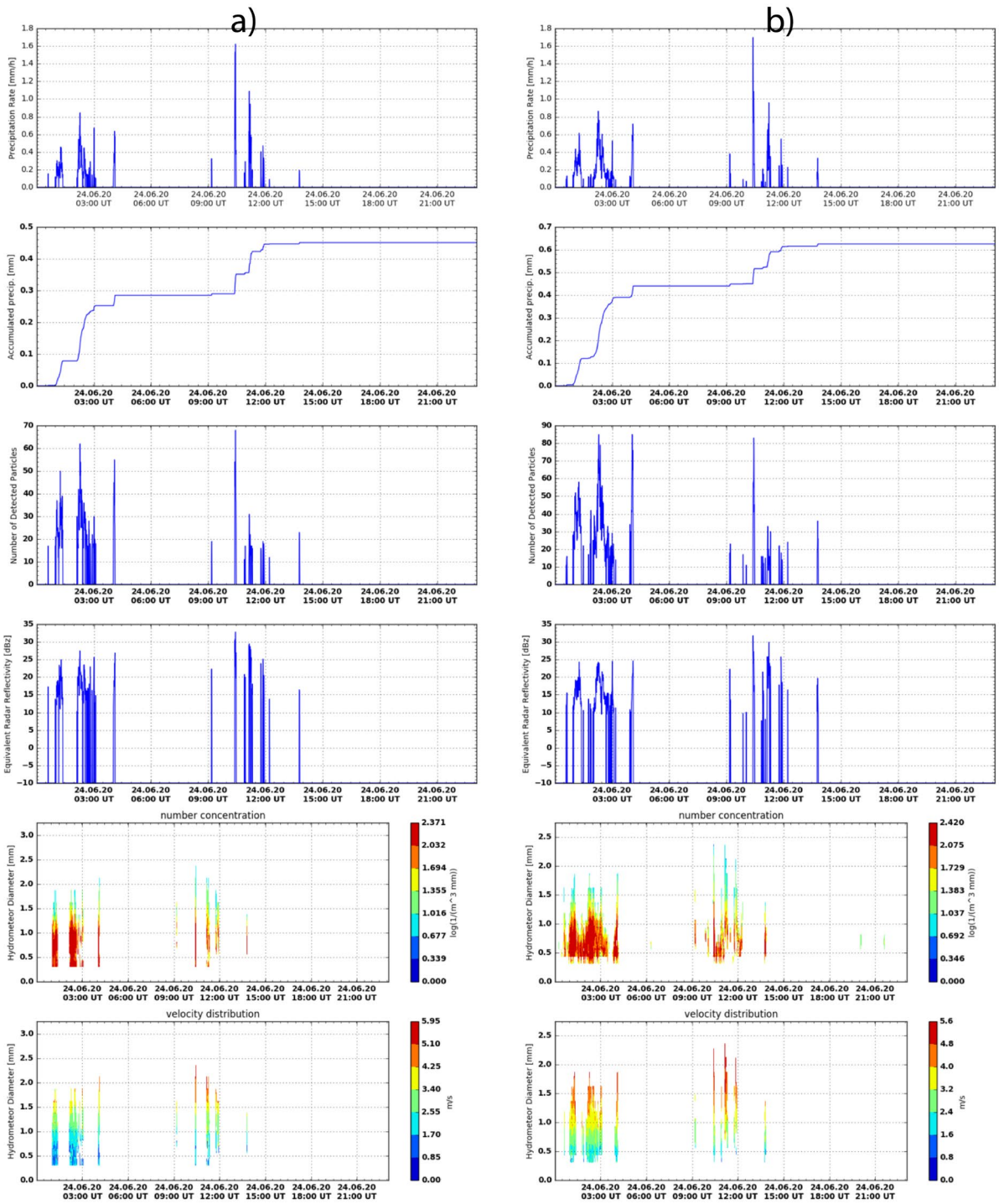

Fig. 3: Parsivel-2 laser disdrometer output (not quality assured) measured on 24 June on the bow crane (column b) and on the OCEANET container (column b).

Leg 4 was dominated by low overcast or fog conditions (e.g., Fig. 4) largely preventing full tropospheric lidar profiling. A first assessment of profiles at clear sky conditions showed that pronounced upper tropospheric aerosol layers were less frequent than during previous legs. In depth analysis of the lidar profiles still needs to be done.

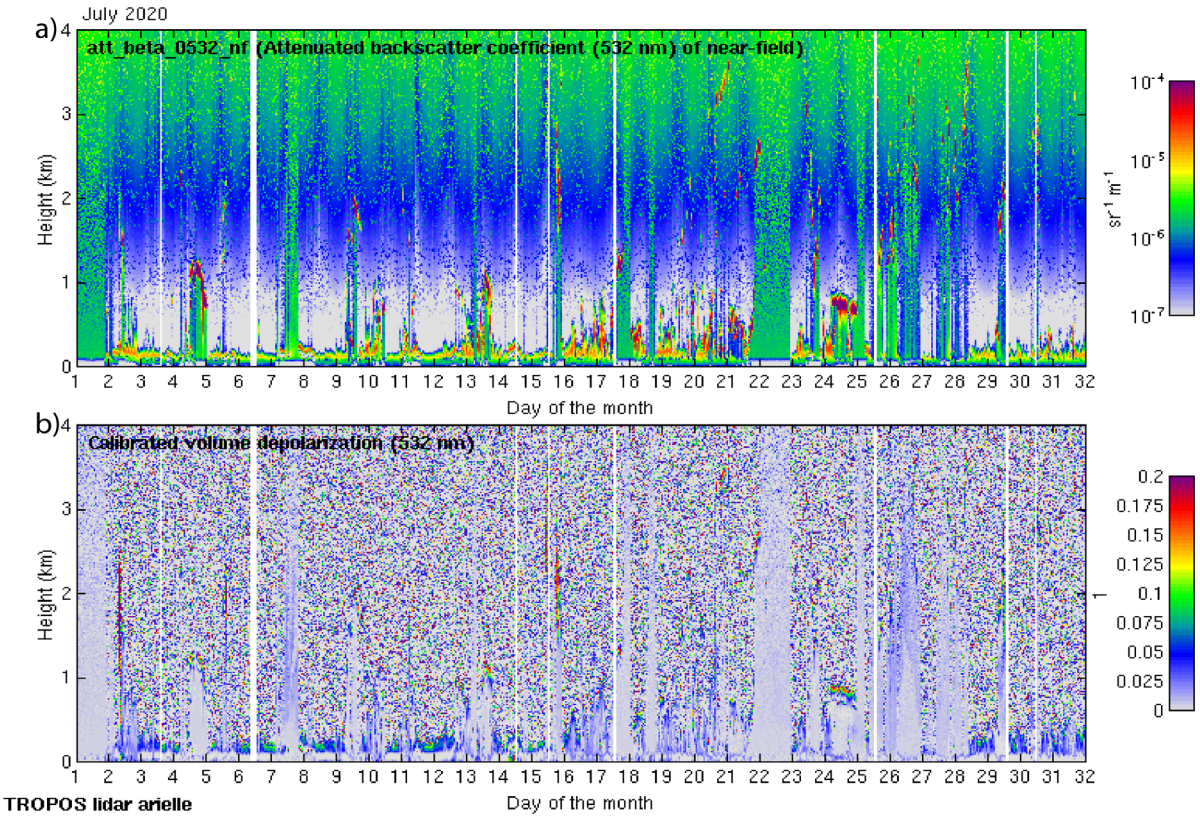

Fig. 4: Temporal development of a) the attenuated backscatter coefficient (near field) and b) the volume depolarization ratio at 532 nm wavelength during July 2020 measured by OCEANET Arielle PollyXT lidar on the bow of *Polarstern*.

Data management

All data are handled, documented, archived and published following the MOSAiC data policy (see APPENDIX). The raw data from the OCEANET platform are stored in the MCS following the MOSAiC data policy. The Polly^{XT} lidar data and quicklooks will be processed and made available through PollyNET (http://polly.tropos.de). Data will be stored at the PANGAEA data repository (World Data Center PANGAEA Data Publisher for Earth & Environmental Science www.pangaea.de.

References

Baars, H. et al. (2016) An overview of the first decade of PollyNET: an emerging network of automated Raman-polarization lidars for continuous aerosol profiling, Atmos. Chem. Phys., 16, 5111–5137.

Bohlmann, S. et al. (2018) Ship-borne aerosol profiling with lidar over the Atlantic Ocean: from pure marine conditions to complex dust–smoke mixtures, Atmos. Chem. Phys., 18, 9661–9679.

Engelmann, R. et al. (2016) The automated multiwavelength Raman polarization and water-vapor lidar PollyXT: the neXT generation, Atmos. Meas. Tech., 9, 1767–1784.

Illingworth, A.J. et al. (2007) CloudNet: Continuous evaluations of cloud profiles in seven operational models using ground-based observations, Bull. Amer. Meteor. Soc., 88, 883-898.

Kanitz, T. et al. (2013) North-south cross sections of the vertical aerosol distribution over the Atlantic Ocean from multiwavelength Raman/polarization lidar during Polarstern cruises, J. Geophys. Res. Atmos., 118, 2643-2655.

Kanitz, T. et al. (2011) Contrasting the impact of aerosols at northern and southern midlatitudes on heterogeneous ice formation, Geophys. Res. Lett., 38, L17802.

Yin, Z. et al. (2019) Aerosol measurements with shipborne sun-sky-lunar photometer and collocated multiwavelength Raman polarization lidar over the Atlantic Ocean, Atmos. Meas. Tech., in press.

3.4. ATMOSPHERIC SURFACE FLUXES FOR UNDERSTANDING SEA-ICE THERMODYNAMICS AND DYNAMICS

Matthew Shupe[1,2], Jackson Osborn[1,2]

(not on board:) Ola Persson[1,2], David Costa[1,2], Thomas Ayers[2], Christopher Cox[2], Christopher Fairall[2], Michael Gallagher[1,2], Daniel Gottas[2], Jesse Leach[2], Sara Morris[2], Sergio Pezoa[2], Taneil Uttal[2], Ian Brooks[3], Jennifer Hutchings[4], Don Perovich[5], Timothy Stanton[6], Roberta Pirazzini[7]

[1]EDU.CU
[2]GOV.NOAA
[3]UK.UNI-LEEDS
[4]EDU.ORSU
[5]EDU.DARTMOUTH
[6]EDU.NPS
[7]FI.FMI

Objectives:

This project is designed to examine the Surface Energy Budget (SEB) and how it impacts the sea-ice thermodynamic and dynamic processes that control the state of the ice over a full year. The PS122/4 collection period captured the onset of melt and the development of the melt season, as well as the movement of the MOSAiC floe to the ice edge region where it suffered substantial degradation and eventual collapse. In combination with partner MOSAiC projects, the overarching project objectives include:

(a) Build comprehensive atmospheric SEB, sea ice energy, upper ocean heat, and sea-ice momentum budgets; examine how these co-vary in space and time over all seasons of the year; and develop temporally-evolving process relationships among multiple key parameters.

(b) Use detailed field observations and a coupled regional model to examine how energy transfer processes (thermodynamics) are influenced by sea-ice deformation (dynamics) on sub-seasonal to seasonal time scales.

(c) Assess sea-ice predictability related to dynamic and thermodynamic process relationships, using a full year of quasi-operational, 10-day sea-ice forecasts.

In support of these broad project goals, the specific objectives of the SEB Flux team during PS122/4 was to continue the partial observations that had been left running on the sea ice from the PS122/3, to re-establish observations on the ice pack at a new Central Observatory, and provide partial operational support for a number of related guest programs that did not have representatives on-board during PS122/4.

This project is funded by the US National Science Foundation and the US National Oceanic and Atmospheric Administration.

Work at Sea

Work during PS122/4 for the SEB Flux Team had four components: (1) Maintain, fix, and re-deploy two Atmospheric Surface Flux Stations (ASFS) for use in the Distributed Network and elsewhere; (2) Re-establish a Met City domain for the new Central Observatory including installation of the 11m tower; (3) Installation, maintenance, and demobilization of a number of partner projects at various locations, including recovering of various assets from the Distributed Network. PS122/4 started on 6 June in Svalbard with the transfer of all scientific crew from the *Sonne* and *Maria S. Merian* vessels onto *Polarstern* followed by an extended

voyage north into the pack ice towards the original MOSAiC installation. It ended on 10 August with the transfer of personnel to the *Akademik Tryoshnikov* after a rendezvous and resupply in the Fram Strait. All parameters measured, including their installation location, are outlined in Table 3.4.1.

Atmospheric Surface Flux Stations

At the start of Leg 4 this project only had one operational system in the MOSAiC constellation, but it was an important one to maintain the timeseries of surface energy budget measurements at the MOSAiC Central Observatory. Flux station ASF30 had been moved during Leg 3 into the Central Observatory and it was left there near the former Ocean City to operate while *Polarstern* left the region to go conduct a crew rotation near Svalbard. During the absence, ASFS30 communicated via Iridium satellite back to *Polarstern*, providing summary data of the observations. Importantly, this station was in place as the surface transitioned towards melt and ultimately reach the onset of the melt season (see preliminary results below). ASFS30 had been left in a somewhat weakened state as the power system was not operating at full efficiency and thus the fast water vapor instrument was turned off during this time. The system operated well during the full period that *Polarstern* was away from the MOSAiC floe. Upon arrival at the MOSAiC floe, ASFS30 was observed aerially from helicopter surveys on 15 June and appeared to be safe and stable. The site was first physically visited on 21 June, including basic maintenance, re-fueling, and the installation of a new methanol fuel cell for power generation. On 30 June, ASFS30 was slingloaded via helicopter back out to the L2 site in the Distributed Network, where it could re-join other buoy systems including the SIMB3, AOFB, ITP, and Snow buoy installed there. A new position was found wherein the ASFS30 was now installed more than 20m away from the AOFB while it had previously been less than 10m away. The site was visited again on 14 July for basic maintenance and to fix a couple of continuing issues. Over time, the L2 site drifted southward much slower than the main MOSAiC Central Observatory and eventually the radio communications link was insufficient to span the more than 40 nautical miles between sites, such that ASFS30 communicated with *Polarstern* only via Iridium satellite communications. Eventually towards the end of July, the drift brought the L2 site back closer to the *Polarstern*, allowing for renewed radio communications and the transfer of much of the data. ASFS30 was removed from the L2 site on 2 August via a short helicopter sling load, a day or two before that ice floe entirely fell apart. Overall, the ASFS30 operated continuously from before Leg 4 began through 2 August, except for the couple of brief hours that it was shut down for the helicopter sling loads.

Upon embarkation on Leg 4, ASFS50 was onboard the working deck of *Polarstern*. During transit the system was fixed in many ways, including installation of a refurbished sonic anemometer, a new set of flux plates, and a new methanol fuel cell. The station was run onboard *Polarstern* during the transit to ensure its robust operations. After arrival at the final parking position, ASFS50 was lifted down to the ice on 24 June and operated within the logistics area until a suitable installation site could be determined. During this period the system operated but the installation conditions were not appropriate for rigorous scientific measurements. On 29 June the system was manually pushed over the ice into a position near the interface of the Second Year Ice (SYI) and the First Year Ice (FYI) parts of the MOSAiC floe, near the ROV domain (see Figure 3.4.1). It was pointed out into the FYI domain direction and towards the edge of the floe, but was just more than 200m from the floe edge (see map in Fig. 3.4.1). Initially the sled was installed on top of a shallow ridge to provide stability over a rapidly evolving and melting surface. However, the sled was slightly adjusted on 4 July by pushing it forward a couple of meters to improve the field of view of the downward looking instruments. This adjusted view looked down on melting ice, but evolving melt ponds were visible approximately 1-2m to the left and 3-4 m to the right when looking out the sled radiometer boom (see Fig. 3.4.2 for the approximate field of view of the downlooking radiometers). The general objective of the installation at this FYI site was to

provide for a representative view of the thinner ice domain that would provide a nice complement to the observations at Met City, which were over thicker, more rugged SYI. ASFS50 was visited every couple of days to maintain the radiometers in good level and to manage the snow ablation. The system operated consistently until it was removed on 30 July. During this extraction from the ice the sled was pushed by a team of people over rough surfaces and through a melt pond that was perhaps 30cm deep. After this point in time, the station was secured on the *Polarstern*.

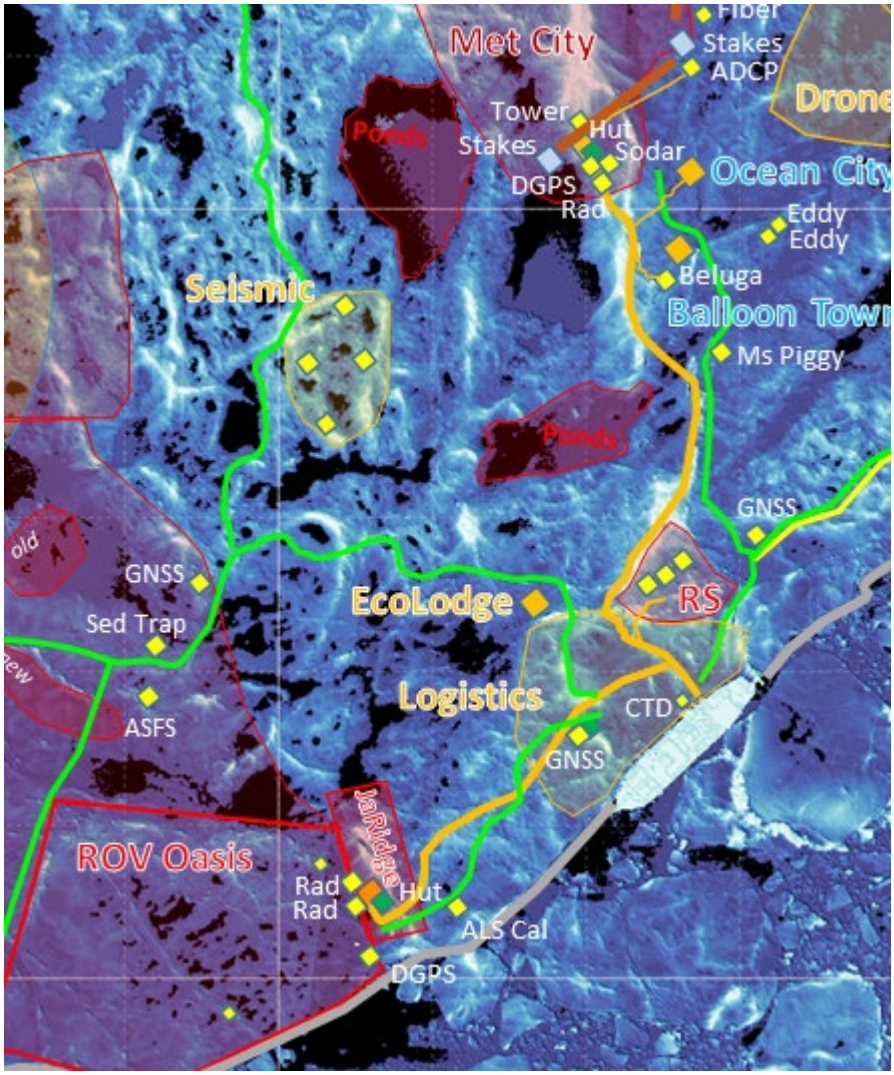

Fig. 3.4.1: Zoomed in map of the middle part of the MOSAiC Central Observatory during Leg 4. Extending out from the ship are power lines (orange) and trails (green) with various installations on the ice (yellow, orange, blue, and green diamonds). The Met City area is labelled in the upper center, including the (11m) tower, Met Hut, and sodar referred to in this report. The ASFS50 is visible in the lower left side of the map. The FMI radiation suite was located at the bottom of this map as the bottom yellow diamond labeled „Rad“.

Fig. 3.4.2: Fisheye photograph looking down near the radiation measurements at ASFS50 in the FYI area on 26 July 2020. The primary view is of melting ice, however, melt ponds were within the viewed area. This photograph also demonstrates the direct reflection effect of the sun off of melt ponds.

In addition to the operations on the sea ice, after recovery of both stations they were installed adjacent to each other onboard *Polarstern* on the rear working deck. While the measurements at this time onboard cannot all be considered relevant for the natural environment, they do provide an opportunity for a comparison data set between these two stations that will help in cross referencing the measurements during post processing and quality assurance.

Met City

Upon arrival at the MOSAiC floe on 17 June, the remaining floe was surveyed and explored. Based on these explorations we identified an appropriate parking position and moved the ship to that location. On 20 June we identified a stable spine for MOSAiC utilities and a location on top of one of the floe's higher ridges for Met City about 400m to the north of the ship (see Figure 3.4.1). While operating from a ridge is not ideal for measuring atmospheric turbulence, the condition of the ice surface at the time of this installation was sloppy, wet and melty such that there were few locations that would provide the stability needed for large infrastructure like a hut, power lines, and an 11m tower. Thus, the ridge line was chosen. Flat areas were carved out for the base of the tower and the Met Hut. Then over the following days, the basic infrastructure was put in place. During this time the base of the tower was installed, tower sections assembled, and all instrumentation fastened to the tower (see table of measurements made). The Met Hut (formerly Remote Sensing Hut) was flown into place via a helicopter slingload. By 25 June the tower was mostly assembled and operational in the down position, providing for a period of intercomparison of the different instruments. Guy lines were set in three angles, with the primary line being attached to the Met Hut, and two other lines being through-ice anchors, passing through more than 5m of ice in the area. On

27 June, with the help of a large team, the tower was lifted vertically into place, marking the start of full scientific operations. Overall, the set up and operation of the tower was identical to those during the previous installation at the original Met City with the primary exception being that the Licor fast water vapor sensor was installed at the nominal 6m height instead of the nominal 2m height. Also, the nominal 2m Met boom was lowered somewhat on the tower because the tower base was above sea-level. While difficult to determine exactly, we estimate that the base of the tower was at about 1.5-1.8m above sea level.

Operations of Met City and the met tower were fairly consistent over time. During the first couple weeks of operation there were about 4 power outages, primarily due to polar bears messing with the power lines and once because the ship was being pushed off of its position. Otherwise, the line power was consistent in time and scientific operations were un-interrupted. No fiber optic cable was run, but a wireless LAN was provided at the Met Hut for connecting equipment. This allowed for the transfer of most data and remote connections to equipment as needed to support standard operations. The largest challenge for tower operations was ablation of the snow and ice. At an early stage ablation shields were constructed and installed around the base of the tower and the Met Hut. These worked very well to limit melt but there was still substantial melt from under the tower, requiring additional snow/ice to be shoveled onto the base of the tower every 1-2 days. Over the course of operations there was no indication of instability in the base, and the tower remained steady in its position for the full time. On 29 July the tower was stopped, lowered, and dis-assembled all in one day along with most of the rest of Met City. Within two days the floe then totally disintegrated.

During the 32 days of tower operations, most instruments remained in ideal operation status. There was very limited icing observed on instruments, only during one freezing drizzle event. Some instruments were impacted by the accumulation of liquid water precipitation, leading to periodic poor data quality on the Licor fast water vapor sensor. These issues generally resolved themselves quickly. The flux plates were installed on the original west side of the tower at the interface of the snow and the ice. Over time these melted out entirely and were periodically re-buried under the melting ice layer; due to substantial direct solar heating effects, it is not clear what the flux plate measurements represent under these conditions. Additionally, the surface view of the tower infrared thermometer and sonic ranger (i.e., surface height) were on a sloped surface on the side of the ridge, which will lead to challenging interpretations of the data. The Met City area was generally a busy location, with many other installations set up near Met City that could have influenced the local flow and turbulence (i.e., Ocean City, stake arrays, eddy sleds, and more). Typically, the winds were from favorable directions that would limit impacts and activities on ice were managed in a way as to minimize other work in the upwind direction from the tower, but some influences might be embedded in the data. Careful directional analysis is necessary when considering the tower data. Furthermore, the environmental conditions around the tower were of interest to the measurements. Already at installation there were sizeable melt ponds on both sides of the Met City ridge. Over time these evolved, grew, formed drainage channels, and drained, leaving fewer but deeper ponds (see Figure 3.4.3, which shows many of the installation details).

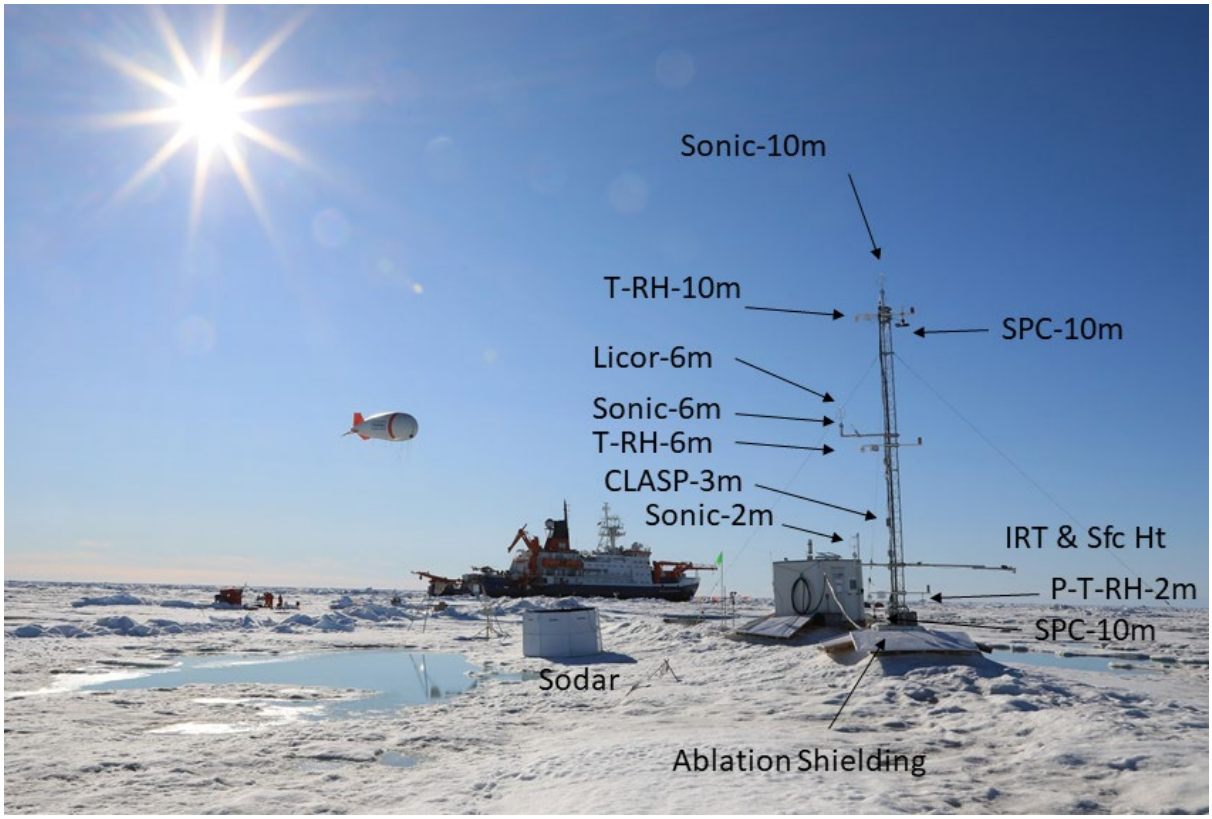

Fig. 3.4.3: Annotated photograph looking south towards Met City and *Polarstern* on 22 July 2020. The instruments are all labeled on the 11m tower. Melt ponds can be seen to either side of the installations.

Support for Partner Projects

During operations of Leg 4, the University of Colorado / NOAA flux team supported the operations of a number of other collaborators whose instruments provide complementary information towards achieving shared scientific objectives. These include:

- SODAR (PI: Ian Brooks): The University of Leeds sodar system is designed to measure wind profiles over the lowest 200-400m. It was set up at Met City starting on 5 July and was operational on 6 July. This system was just to the east of the Met Hut, slightly carved into a sloping surface (see Fig. 3.4.3). The system was leveled and oriented such that the systems NE-to-SW corners were pointed directly at the bridge of *Polarstern*, with NE away. The north side of the system was pointed to approximately 310 degrees upon installation. At set up there were a couple of faults with a couple of the system's transducers but the PI indicated that this would not significantly impact the measurements. The sodar operated consistently when there was power provided to Met City, routinely showing wind profiles on its laptop up to multiple 100s of meters. Upon take down of systems on 29 July, the sodar transmitter was found to have slipped sideways and significantly out of level and it is not clear when this occurred.
- FMI-Radiation (PI: Roberta Pirazzini): A radiation suite from the Finnish Meteorological Institute was designed to measure the upwelling, downwelling, longwave and shortwave radiation, including the partitioning of direct and diffuse shortwave radiation. It was set up and maintained near the ROV installation on the FYI part of the floe (see map in Figure 3.4.1 and photo in Figure 3.4.4), with full operations starting on 10 July. During initial set up it was found that the system's battery had failed and so a replacement battery was found and installed. Additionally,

the guy anchoring system and guy wires used to level the system were not sustainable in a melting environment as they would melt out of place within about a day. Thus, after some days of operation wherein the system would become very out-of-level very rapidly, the anchoring system was changed to anchors that extended through the ice (>1m thick ice) on 19 July, which allowed for the system to remain much more level thereafter. The system was uninstalled on 28 July as conditions near ROV were becoming less stable and the PI did not want to continue to risk the system. During the period of operations, the system was consistently functioning, although periodically it was so far out of level to be effectively not useable. The field of view of the radiometers evolved in time as the local melt ponds expanded.

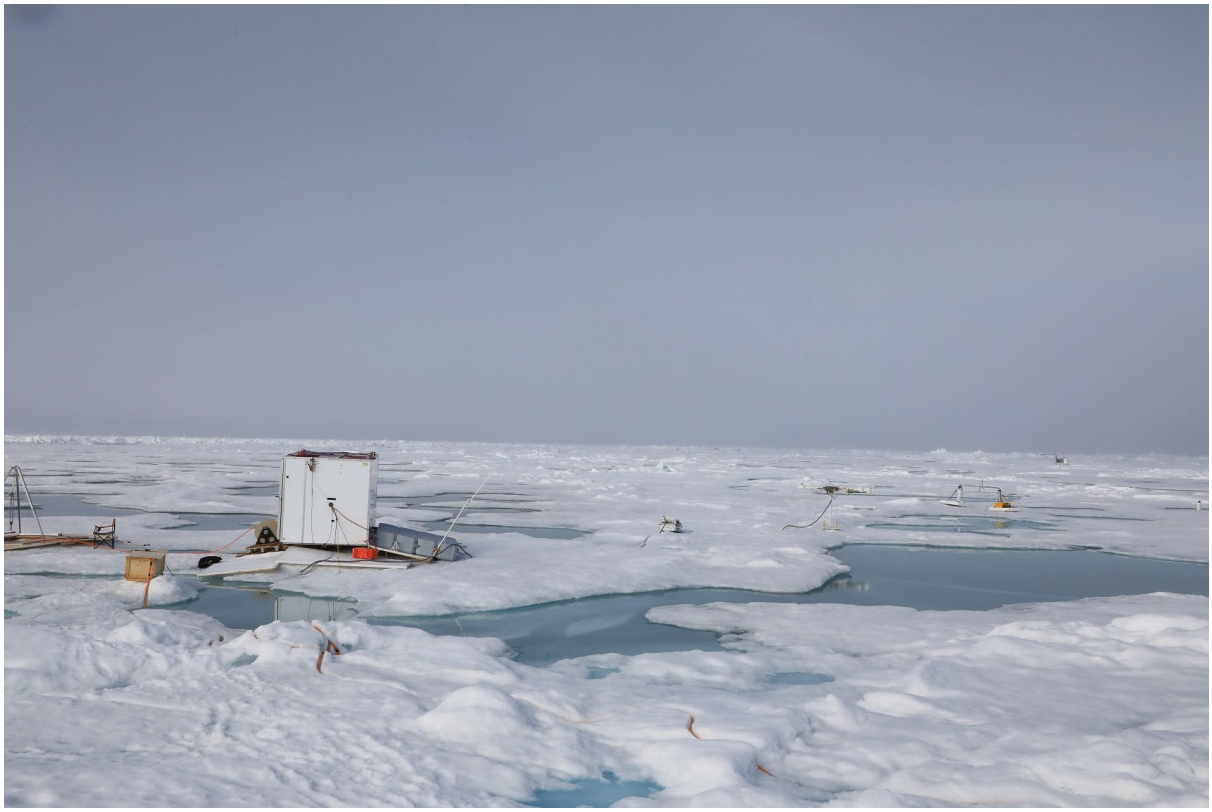

Fig. 3.4.4: Photograph looking westward into the ROV area on 21 July with the FMI radiation suite visible about 15m to the right. Directly under the radiation suite was melting ice, however melt ponds were in the lateral view.

- Snow Particle Counters and CLASP (PI: Markus Frey). The British Antarctic Survey provided sensors for installation on the 11m tower to measure blowing snow particles and aerosols. The CLASP was operated at approximately 3m height. The two SPCs were operated at about 30cm and 10m (see Figure 3.4.3). These were installed with the original tower installation. For the first few days the CLASP had a few issues with communications, maintaining only periodic connection to the data logging system. Eventually the spare CLASP system was installed which enabled more consistent operations. The SPCs functioned well but there was one multi-day period of observations missed on one of the systems due to an improperly installed data card. There was very limited ice phase precipitation during Leg 4 and thus relatively little for the SPCs to observe. The lowest SPC might have been impacted by low-level turbulence and flow distortion around the base of the tower.

- Ice Video Camera System (PI: Max Maahn): The VISSS takes high resolution, rapid succession photographs of falling ice crystals, and was installed at the end of Leg 3 on the Observation Deck of Polarstern to provide stability for longer term operations. In this position it could suffer from potential flow distortion on the trajectory of falling precipitation, but would not be challenged by cracking and moving ice on the surface. Operations were consistent during Leg 4, however there was very little precipitation or snowfall to measure.
- Distributed Network: Across the Distributed Network key partners have installed equipment that is very relevant for our understanding of the surface energy budget, energy fluxes to the sea ice, and more. During the recovery phase of Leg 4, Polarstern journeyed across the Distributed Network domain and retrieved various installations. The atmospheric flux team led the recovering of the Arctic Ocean Flux Buoy and Seasonal Ice Mass Balance Buoy from L2, as these will hopefully be re-deployable during Leg 5. Additionally, the team supported recovering of ice tethered profilers, although these will not be re-installed.

Tab. 3.4.1: Parameters measured and systems maintained by the SEB/Flux team during Leg 4. "Near continuous" measurements at Met City means that the measurements were operational except for the relatively short power outages that occurred on a few occasions.

Variable	***Instruments***	***Installation Locations***	***Details***
Surface Conductive Heat Flux (at ice snow interface)	*Hukseflux Flux plates*	*Near 11m tower at Met City (2)*	*Data often questionable in summer due to melt out and solar heating.*
		ASFS50 at FYI area (2)	*Data often questionable in summer due to melt out and solar heating.*
		ASFS30 at Old CO and then L2 (2)	*At Old CO from 6-30 June and thereafter at L2 until 2 August. Data often questionable in summer due to melt out and solar heating.*
P, T, RH – 2m	*Vaisala PTU337*	*11m tower at Met City*	*Operated continuously for 27 June through 29 July.*
		ASFS50 at FYI area	*Operated continuously for 29 June through 30 July.*
		ASFS30 at Old CO and then L2	*At Old CO from 6-30 June and thereafter at L2 until 2 August.*
T, RH – 6m & 10m	*Vaisala HMT307*	*11m tower at Met City*	*Operated continuously for 27 June through 29 July*
Fast response winds – 2m, 6m, and 10m	*Metek Sonic anemometer*	*11m tower at Met City*	*Operated continuously for 27 June through 29 July*
Fast response winds – 3m	*Metek Sonic anemometer*	*ASFS50 at FYI area*	*Operated continuously for 29 June through 30 July.*
		ASFS30 at Old CO and then L2	*At Old CO from 6-30 June and thereafter at L2 until 2 August.*
Fast water vapor and carbon dioxide – 6m	*LICOR open path gas analyzer*	*11m tower at Met City*	*Operated continuously for 27 June through 29 July. Periodic data degradation due to buildup of moisture on sensor.*

Fast water vapor and carbon dioxide – 3m	*LICOR open path gas analyzer*	*ASFS50 at FYI area*	*Operated continuously for 29 June through 30 July. Periodic data degradation due to buildup of moisture on sensor.*
		ASRS30 at Old CO and then L2	*At Old CO from 6-30 June and thereafter at L2 until 2 August. Periodic data degradation due to buildup of moisture on sensor.*
Position and Heading, 2m	*Hemisphere dual GPS*	*11m tower at Met City*	*Operated continuously for 27 June through 29 July*
		ASFS50 at FYI area	*Operated continuously for 29 June through 30 July*
		ASFS30 at Old CO and then L2	*At Old CO from 6-30 June and thereafter at L2 until 2 August.*
Surface height (snow depth, ice melt)	*Campbell SR50 sonic ranger*	*11m tower at Met City*	*Operated continuously for 27 June through 29 July*
		ASFS50 at FYI area	*Operated continuously for 29 June through 30 July*
		ASFS30 at Old CO and then L2	*At Old CO from 6-30 June and thereafter at L2 until 2 August.*
Infrared Surface Temperature	*Apogee IRT*	*11m tower at Met City*	*Operated continuously for 27 June through 29 July. Indications of solar influence on measurements.*
		ASFS50 at FYI area	*Operated continuously for 29 June through 30 July. Indications of solar influence on measurements.*
		ASFS30 at Old CO and then L2	*At Old CO from 6-30 June and thereafter at L2 until 2 August. Indications of solar influence on measurements.*
Radiation: SW, LW, up and down, 2m	*Hukseflux radiation suite*	*ASFS50 at FYI area*	*Operated continuously for 29 June through 30 July.*
		ASFS30 at Old CO and then L2	*At Old CO from 6-30 June and thereafter at L2 until 2 August.*
Radiation: SW, LW, up & down, SW diffuse & direct	*Radiation Station (FMI)*	*Near ROV installation.*	*Operated continuously from 10-28 July. Some data quality issues related to tilting of radiation stand.*
Aerosol size distribution – 3m	*CLASP (BAS)*	*11m tower at Met City*	*Operated continuously for 27 June through 29 July, with some interruptions in first days w/ communications issues.*
Snow Particle Counts – 0.3 and 10m	*SPC (BAS)*	*11m tower at Met City*	*Operated continuously for 27 June through 29 July.*
Wind Profiles (u,v,w up to about 400m)	*SODAR (U. Leeds)*	*Near Met Hut*	*Operated continuously from 6-29 July. Unquantifyied period of questionable data due to tilting transmitter.*

Ice Crystal Precipitation Images	*VISSS (U. Colorado)*	*Polarstern Observation deck.*	*Operated nearly continuously from early July through the rest of Leg 4.*

Preliminary (expected) results

Measurements made as part of this project have extended important timeseries that include high-quality estimates of atmospheric surface heat and momentum fluxes at multiple locations across the MOSAiC domain and the lower atmosphere structure at the MOSAiC Central Observatory. Ultimately these fluxes will be combined with project partner measurements of ocean heat fluxes, sea ice thermodynamic state and thickness, and regional-scale sea-ice movement and deformation to understand the dynamic and thermodynamic drivers of the sea-ice life cycle. While there are many expected results and applications of the data, a few are highlighted here to demonstrate the detail and breadth of the obtained data sets.

The first area of focus is the onset of melt. This transition technically occurred prior to the start of Leg 4, but it sets an important foundation for the observations during the rest of the melt season. Figure 3.4.5 shows eight days of observations from ASFS30 while it operated at the Old MOSAiC Central Observatory while the Polarstern was away to manage the rotation from Leg 3 to Leg 4. The top panel shows the evolution of surface temperature (red), initially having diurnal variability at temperatures colder than 0°C, but then on 25 May reaching 0°C and staying at the melting point as excess energy at the surface went into snow melt. Air temperatures at 2m height (panel 2) show similar variability with air temperatures reaching above 0°C during the surface melting period.

The third panel shows the longwave (LW) radiative fluxes at the surface. Initially there were periods of clear sky (LWU-LWD is on the order of 60 W/m^2) and periods of cloudy skies (LWU-LWD is on the order of 10 W/m^2). After a prolonged cloudy period on 23-24 May, the atmospheric temperatures warmed such that under cloudy conditions the LWD was actually periodically larger than LWU, indicating the presence of thick clouds and a temperature inversion. At the same time, the shortwave (SW) radiation (4th panel) showed typical diurnal variation with indications of clouds at times. In spite of decreasing SWD towards the melt onset, because of clouds, the surface albedo (SWU/SWD) showed a slight decrease of about 5% as a result of surface melting. The decrease in albedo resulted in an increase in absorbed SW radiation of approximately 10 W/m^2. The combined increase in surface radiation due to these two processes contributed significantly to both triggering and driving the surface melting process, pushing the MOSAiC ice floe into the melt season.

To represent much of the Leg 4 data, a subset of preliminary measurements from the flux team for the month of July is plotted in Figures 3.4.6 and 3.4.7. Pressure variations were generally weak, with the largest swings occurring in the first two weeks of July. The second half of July was a relatively stationary pattern and Polarstern sat under a weak high-pressure ridge. Near-surface windspeeds clearly coincided with the variability in large-scale state, with the highest winds experienced during minor low-pressure events during the first part of July, although the peak near-surface winds were only up to 10 m/s. Considering surface radiation, a couple of points are noteworthy. First, clouds were frequent. There were two days, 1 and 22 July, that were mostly clear all day, with smoothly varying downwelling SW radiation over the course of the day and strong deficits in the net LW radiation (LWD-LWU). Otherwise, clear sky periods were intermittent and brief; these can be clearly observed in the second panel of Figure 3.4.7 when LWD is less than about 270 W/m^2. As the month progressed, the incident SW radiation continued to decline with solar midnight values declining from about 80 W/m^2 down to 40 W/m^2 by the end of the month. Interestingly the Net SW radiation (SWD-SWU) remained relatively consistent or even increased over the course of the month as a result of a declining surface albedo.

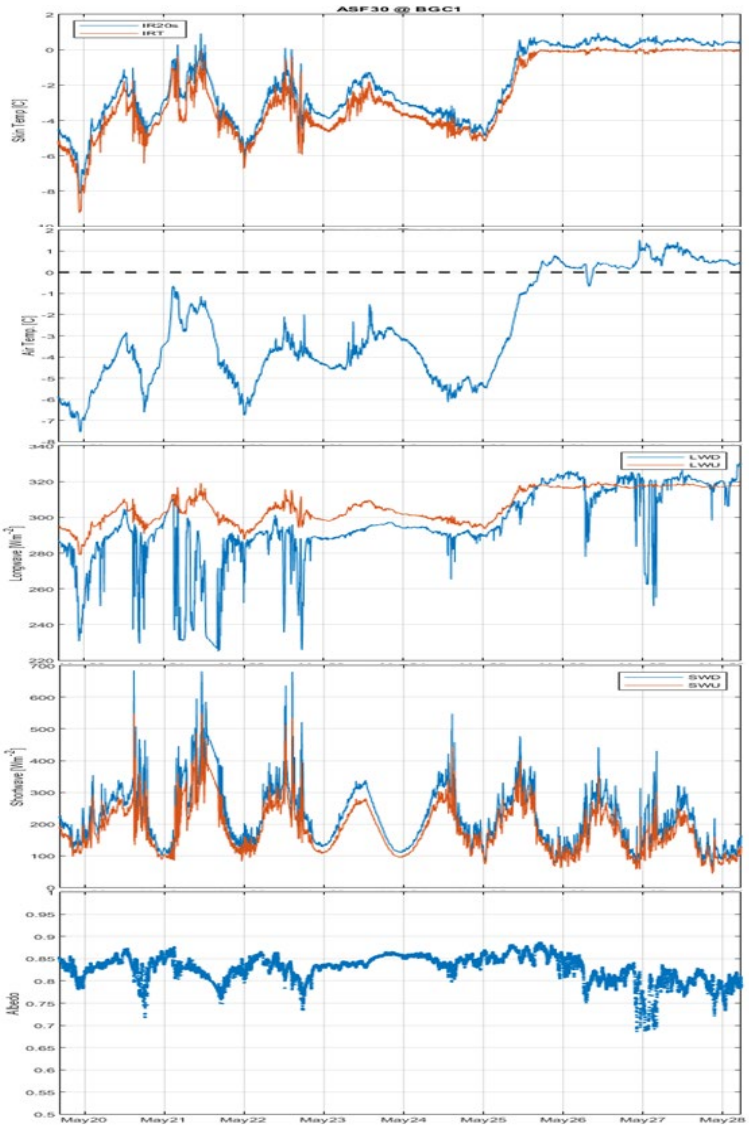

Fig. 3.4.5: Timeseries data in late May 2020 from ASFS30 installed at the Old Central Observatory site near Ocean City, showing the onset of the melt season, including: Surface skin temperatures, 2m air temperature, LWD and LWU, SWD and SWU, and surface albedo.

Being in the middle of the melt season, the surface temperature was typically constant at the melting point, 0°C. During the first two days of the month the surface temperature, as well as near-surface temperatures, dropped significantly below 0C; sub-freezing temperatures also occurred during a couple of brief events towards the middle of the month, the most significant of which occurred on 14-15 July when lower atmosphere temperatures were below -1°C. These periods of colder surface conditions were typically related to clear skies with large negative net LW radiation. However, the two extended clear sky days demonstrate the diurnal interplay of LW and SW radiative processes. During the diurnal solar minimum, the large LW radiative loss at the surface during clear sky periods drove surface temperatures colder. However, as the sun gained elevation towards solar noon the surface temperatures would again climb until the sun started descending again. This same pattern occurred on both 1 and 22 July. The suggestion here is that clouds typically had a warming effect on the surface except for during the diurnal peaks of the solar cycle during this time of year. Atmospheric temperatures showed more variability than the surface temperature, with variability typically between +/-1°C. Only in the last few days of July, when temperatures at

about 200m altitude reached higher than 10°C, did the near-surface temperatures consistently reach above 1°C.

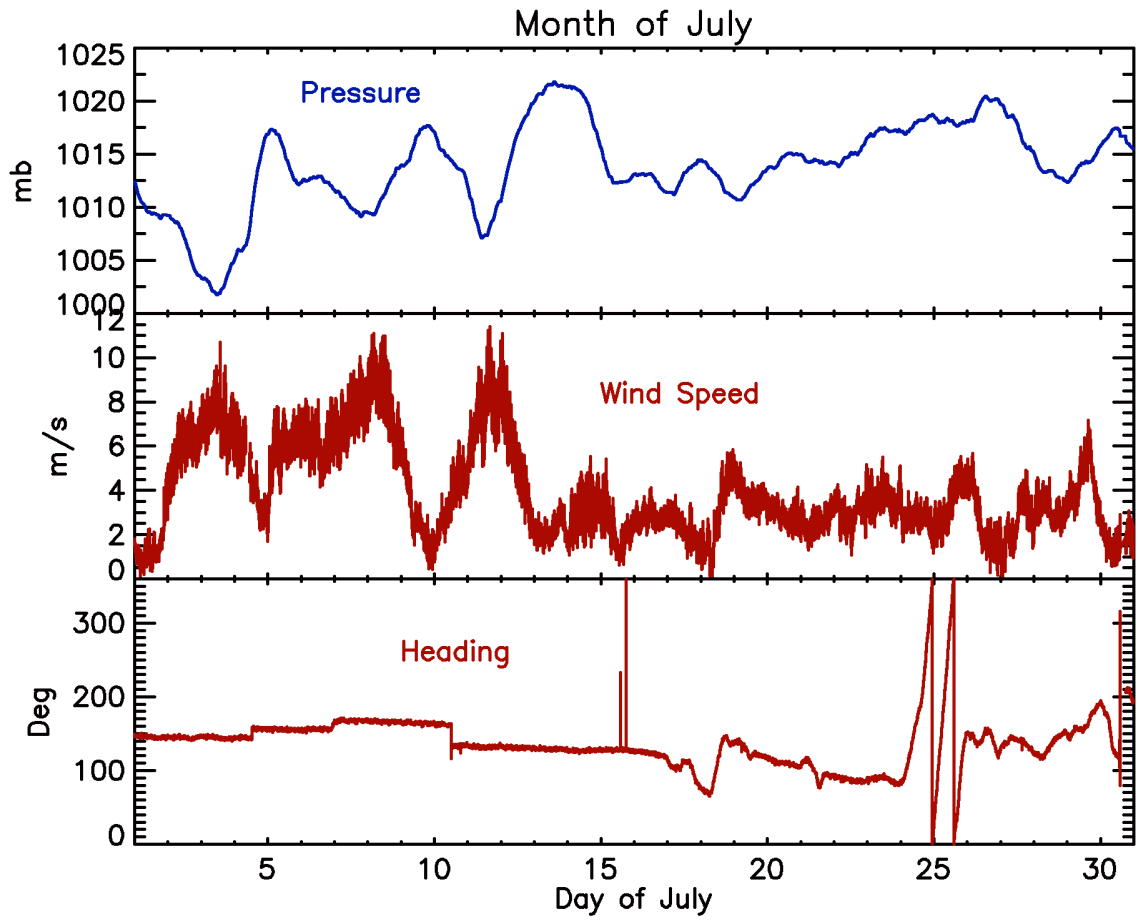

Fig. 3.4.6: Timeseries data from the month of July at ASFS50 in the FYI area of the MOSAiC floe showing atmospheric pressure, 2m wind speed, and the heading.

Lastly, the heading of the main MOSAiC floe is particularly interesting, as shown by the third panel of Figure 3.4.6. The small step changes in the first 10 days of July were due to small adjustments to the ASFS50 as the surface ice melted. During most of this time the station had a heading around 120-150 degrees. During the second half of July as the MOSAiC floe drifted into the Fram Strait and the ice pressure began to decrease the heading started to change more rapidly, moving by 30-60 degrees over short periods with a general tendency towards a counter clockwise rotation. Then on 24 July the floe began to spin. Over the course of two days the floe spun about 770 degrees clockwise, before settling down again with a heading near 150 degrees.

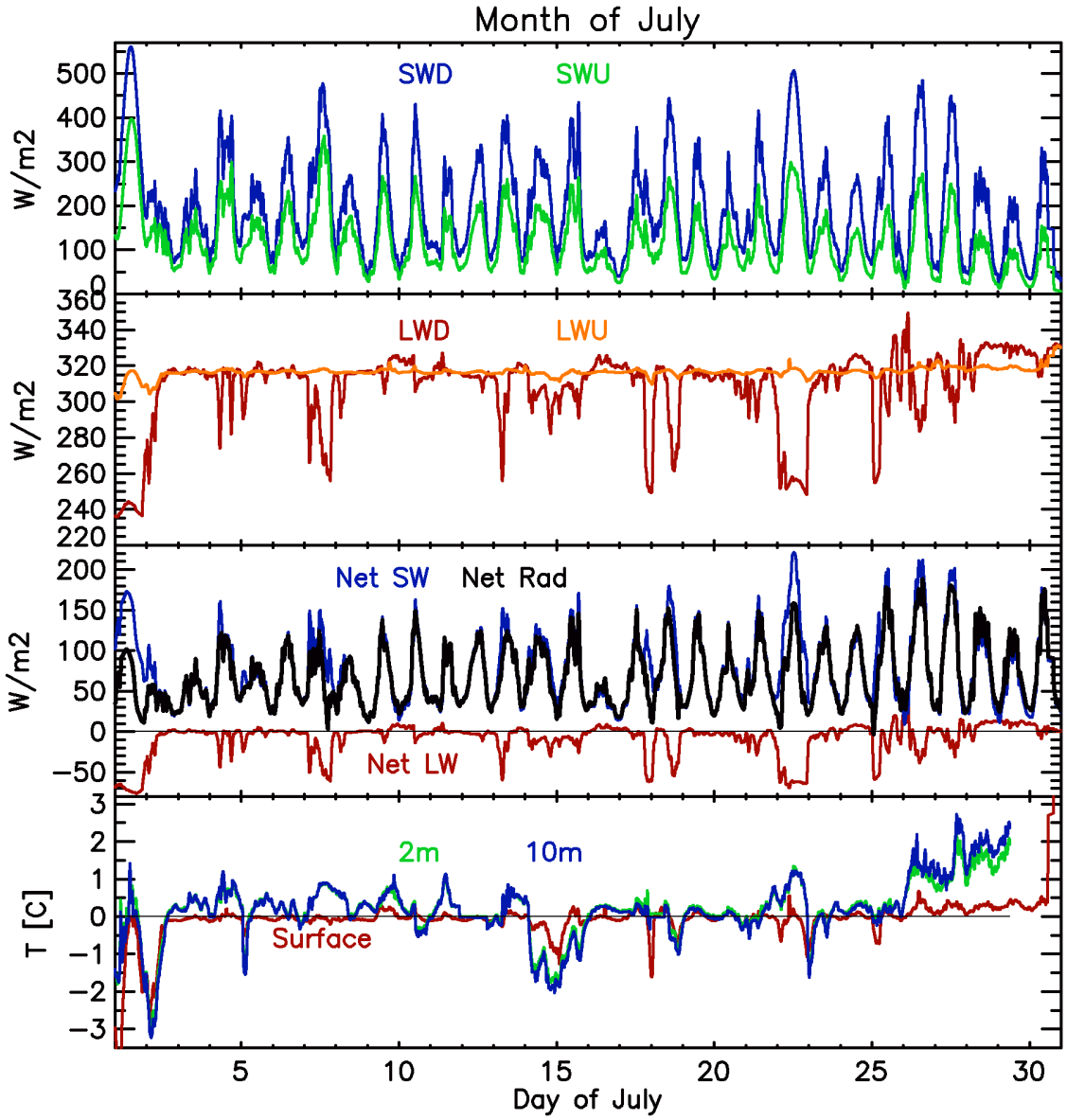

Fig. 3.4.7: Timeseries data from the month of July at ASFS50 in the FYI area of the MOSAiC floe, along with some data from the 11m tower at Met City, including: SWD and SWU, LWD and LWU, Net SW and Net LW radiation along with the total net Radiation, surface temperature, and 2m and 10m air temperatures.

Data management

Data produced at the Met City installation are archived locally in Met City and duplicated in the flux laboratory container onboard *Polarstern*. Data produced at the remote ASFS sites are archived locally on the remote systems; some sub-set of this data is transferred to *Polarstern* via a combination of radio or Iridium modems. The full set of ASFS site data is transferred to *Polarstern* after routine site visits. All data is redundantly archived on the server in the flux laboratory container onboard *Polarstern*. Additionally, a copy of all raw data has been uploaded to the MOSAiC Central Storage onboard *Polarstern*; this data has not yet undergone detailed quality assurance and calibration. Long term archival of quality-controlled data will be done at the Arctic Data Center (ADC) archive, according to the protocol agreed

upon between the ADC and PANGAEA. DOIs for the data will be communicated to PNAGAEA for later access via the future MOSAiC Data Portal. All data are handled, documented, archived and published following the MOSAiC data policy. Exceptions will to be documented in written agreements between the data provider and the MOSAiC Project Board and data manager.

References

None.

3.5 TROPOS TETHERED BALLOON

Michael Lonardi[1], Christian Pilz[2]
(not on board) André Ehrlich[1], Heike Kalesse[1], Andreas Macke[2], Holger Siebert[2], Birgit Wehner[2], Manfred Wendisch[1]

[1]DE.Uni-Leipzig
[2]DE.TROPOS

Objectives

The aim of the Balloon-borne modular utility for profiling the lower atmosphere (BELUGA) is to provide a platform for *in-situ* measurements of the atmospheric boundary layer (ABL). The instruments deployed with the balloon provide data to understand how cloud macro and microphysical properties, together with aerosol microphysical properties, affect the turbulent and radiative energy fluxes as well as the surface net warming/cooling

A 90 m^3 tethered balloon is used to profile of the ABL from the ground level up to 1500 m at cloudy conditions or clear sky, with a payload up to 15 kg. The balloon carries a set of instruments that can be adapted to the scientific aims of the flight and to the weather conditions (see Figure 3.5.1).

BELUGA has been largely deployed in Arctic campaigns with a 90 m^3 balloon on PASCAL (Arctic Ocean, 2017) and a 9 m^3 balloon on PAMARCMiP (Station Nord, Greenland, 2018) and MOCCHA (Arctic Ocean, 2018) [1]. The team operating the balloon during MOSAiC was involved in a test campaign in Jan/Feb 2019 at TROPOS station Melpitz, 40 km east of Leipzig.

The primary interests are:

- gaining a better understanding of stratification and vertical exchange of energy in the Arctic ABL
- investigate the sources and dynamics of aerosol particles and its interaction with clouds

In particular, the research questions formulated for this project are:

- How does the local thermodynamic environment, as compared to remote processes influence Arctic ABL processes?
- Are the locally observed aerosol particle concentrations sufficient to notably modify the microphysical properties and radiative effects of Arctic ABL clouds?
- How do cloud microphysical, radiative, and turbulent processes interact during the life time of mixed-phase clouds in the central Arctic?

The instruments deployed with BELUGA are:

- Standard Meteorology Probe
- CAMP (Cubic Aerosol Measurement Platform)
- Broadband Radiation Package
- Sonic anemometer
- VIPS (Video Ice Particle Sampler)
- HALFBAC (High Volume Aerosol Sampler for Balloon Applications)
- CWS (Cloud Water Sampler)

An additional ozone probe was operated in cooperation with Byron Blomquist (Univ. Colorado – CIRES & NOAA PSL, see Chapter 3.6).

Fig. 3.5.1: Beluga flying with instrument packages.

Work at sea

The required installations for the operation of the tethered balloon on ice were set up from 22 to 25 June at the new Balloon Town site. Multiple skidoo drives with Nansen sledges were taken from the ship to the site to set up the deflection pulley, the winch system, the emergency power generator and 100 m of power cables. The deflection pulley and the winch were secured on ice with 5 steel chains on steel ice anchors below the ice. Required holes were drilled with a 5 cm Kovacs ice drill through ice thicknesses of 3 to 6 m.

With the help of six volunteers from the ATMOS team, the balloon was inflated and set up next to the ship on starboard site between gangway and stern. A 60 m hose was used for the helium filling from racks on-board PS. After filling, the balloon was secured with two ropes to a skidoo and brought to the balloon site. The general parking position of the balloon was on a 30 m rope attached to a chain of 10 m at ground level for polar bear safety.

After two days of stronger winds, the first measurements on two profiles were taken on 29 June. During the second profile, technical problems led to an unintended half deflation of the

balloon. With the help of the nearby team OCEAN the balloon and the instruments were safely brought to the ground and the balloon secured with ice anchors on the ground.

The technical problem was identified as the malfunction of a security valve on the next day. Due to helicopter operations, no refill of the balloon close to the ship was possible in the following days. Single Helium bottles from the AWI tethered balloon team were transported to balloon town to refill the balloon on site on 2 July. The newly sealed helium bottles were insufficient for a complete filling. Not forecasted, rapidly changing weather conditions on the following days made further operations not possible and to prevent the balloon from damage at strong winds, it was completely deflated on 4 July.

After a period of strong winds without any operations, the balloon was again inflated on 9 July next to the ship. The maximum altitude of the profiles taken on 10 July was limited to ca. 600 m due to technical problems with the winch. On the same day, the balloon had to be secured on the ground due to quickly changing wind conditions and a following period of strong winds.

In the morning of 13 July the balloon became operational and profiles were taken in the afternoon. During the second profile the balloon lost helium for unknown reasons but remained stable enough for overnight parking. Another refill at the ship on the next day was necessary to allow for further operations.

Because the AWI small tethered balloon was set up only 60 m away in-between the ship and Balloon Town, the refill operation required 8 volunteers in order to avoid any entanglement when the balloon was brought from Balloon Town to the ship and back.

The balloon became more and more unstable during the next day of operations and couldn't be operated on 16 July. Because of the many technical problems, it was decided to deflate the balloon on 17 July and inflate a spare balloon on 18 July. Work on ice was limited on these days due to polar bear encounters.

Within the next days of operations, the balloon lost a lot of helium and had to be refilled twice until a leakage could be detected and fixed on 23 July.

After more than one week of parallel operations of UAVs and the small tethered balloon, on 22 July coordinated measurements of all airborne platforms of the ATMOS team were made to assess the early morning atmospheric boundary layer dynamics. During the time of operations, the wind directions were highly fluctuant over altitude inducing strong wind shear on the tethers of both balloons. Since both balloons had to be operated with only 60 m clearance to each other, the difficult conditions lead to an entanglement of both tethers. This resulted in a loss of the AWI small tethered balloon, but no scientific instrumentation or the big tethered balloon was damaged.

After another refill in the morning of 25 July and further profiling limited due to a spinning of the complete floe. This introduced a spinning of the ground fixations of both balloons while they are parallel in the air and could have led to another entanglement of tethers.

The work on ice was aborted in the morning of 27 July due to bad visibility and strong winds in combination with thick fog did not allow for any balloon operations on the day after. All work on the ice was ended on 29 July the with the deflation of the balloon and the set down of Balloon Town before the floe broke apart one day after.

Overall, the series of malfunctions of the balloon complicated the logistical operations, resulting in the loss of several hours of flight time and on an intermittent operation during the first part of PS122/4. In addition to that, the available space on the floe was very limited resulting in a very small airspace that had to be shared by all airborne platforms with scientific payloads; e.g. helicopter, big tethered balloon, small tethered balloon and UAVs. All flight operations were well coordinated to allow for an equal share of flight time during general weather conditions with very limited visual flight capabilities. In turn, this resulted in a narrowed scientific plan for BELUGA, with the INP filter sampler and the cloud water sampler not being operated, since the overall needs for quick adaption to rapidly changing weather

conditions could not be met with a stationary balloon on high altitudes for several hours of sampling.

The balloon operated between 29 June and 15 July proved to be able to carry large payloads, up to 17 kg, but needed extensive maintenance due to technical problems. The spare balloon, used from the 19 July onwards, limited the total payload to about 12 kg and therefore narrowed down the possible combinations of instruments but granted profiles on a daily schedule due to the reduced logistical effort to keep the system operational. The payload instruments were largely reliable and suffered minimal failures, and the ability to adapt the payload to the weather conditions allowed to maximize the results from each flight. In addition, measurements received via downlink during the balloon ascents were used to identify important atmospheric features e.g. inversion height or cloud base/top in order to increase sampling resolution and time during balloon descents. The following Table 3.5.1 summarizes the flights performed by BELUGA during PS122/4 and the attached pictures illustrate the mounting of the instruments below the balloon.

Tab. 3.5.1: Profiles with BELUGA and detailed payload. The standard meteorology payload was part of all the flights. In the payload section, a 1 indicates that an instrument was part of the payload while an x indicates if it suffered a partial or total failure.

Date			Start		Stop		Flight#	D-SHIP	Altitude	Payload				
Year	Month	Day	Hour	Minute	Hour	Minute				CAMP	VIPS	BP	SONIC	Ozone
2020	6	29	8	28	9	22	1	45-141	850	1		1		
2020	6	29	12	36	13	55	2	45-156	1200	1		1		
2020	7	10	10	15	11	40	3	46-182	600	1	1			
2020	7	10	12	14	12	28	4	46-183	300			1	1	
2020	7	13	11	54	13	25	5	47-98	1200	1			1	
2020	7	13	13	40	15	15	6	47-99	1500		1	1	1	
2020	7	14	11	40	12	6	7	47-100	1050	1				
2020	7	14	13	29	14	41	8	47-165	850		1	1	1	
2020	7	15	7	51	9	3	9	47-166	1000	1		1		
2020	7	15	11	52	12	51	10	47-167	730		1	1	1	
2020	7	15	12	52	13	10	11	47-168	440		1	1	1	
2020	7	15	13	16	14	42	12	47-169	1000	1			1	
2020	7	19	11	44	12	57	13	47-170	720	1				
2020	7	19	13	5	14	26	14	47-171	720			1		
2020	7	20	8	28	10	18	15	48-126	1300			x		
2020	7	20	13	11	14	48	16	48-127	1050	1				
2020	7	21	7	36	9	3	17	48-128	1050	1		x		
2020	7	21	11	38	13	1	18	48-129	990			x	1	
2020	7	21	13	12	14	55	19	48-130	1050	1				
2020	7	22	3	44	5	5	20	48-131	1020			1		1
2020	7	22	5	12	7	35	21	48-132	1010	1				1
2020	7	23	7	52	8	50	22	48-133	1020			1		
2020	7	23	9	2	10	30	23	48-134	1040	1				
2020	7	23	11	12	12	32	24	48-135	1010			1	1	
2020	7	23	12	33	13	45	25	48-137	1010	x				
2020	7	24	7	41	9	1	26	48-138	1100	1				
2020	7	24	9	6	11	0	27	48-139	1210			1	1	
2020	7	24	11	18	13	0	28	48-140	1180		1	1		

2020	7	24	14	41	14	58	29	48-141	400	1			
2020	7	25	14	6	15	4	30	48-216	1040	1	1		
2020	7	26	12	4	13	31	31	48-217	1000		1	1	1
2020	7	26	13	46	15	0	32	48-218	1070	1	1		1
2020	7	27	7	43	9	0	33	49-98	1015	1	1		

Preliminary (expected) results

Overall, 33 vertical profiles, of which 24 above 1000 m of altitude, were performed in different weather conditions. These include various types of cloud cover (clear sky, fog, clouds in single and multiple layers) and wind conditions (calm or winds >5 m/s from different directions). The profiles were obtained during 14 days of flights, of which 9 were consecutive (19-27 July). The simultaneous operations with a smaller tethered balloon operated by AWI and the UAVs by the University of Colorado Boulder, as well as the 6-hourly radiosounding program (AWI), provides the possibility to compare and supplement some of these *in-situ* data.

A total of 19 aerosol profiles up to 1000 m were performed with CAMP, while the Broadband Radiation Package flew for a total of 21 profiles, of which 18 without failures. The Broadband Radiation Package was deployed together with the Sonic anemometer (9 times), CAMP (7 times) and VIPS (5 times).

Different payload setups were aimed to investigate different properties. The combination of broadband radiation and turbulence offers the possibility to calculate energy fluxes. The use of the Broadband Radiation Package with VIPS was used to assess the impact of cloud microphysics. The combination the Broadband Radiation Package and CAMP was mostly done to make use of the extra payload capability during the operation of the latter, given the limited weight of the Broadband Radiation Package.

The planned co-deployment of VIPS was scaled down due to the reduced occurrence of mixed-phase clouds in this season but the results from this probe are still useful to assess cloud droplet sizes.

- Different weather conditions allowed to conduct a homogeneous investigation of shortwave (SW) and longwave (LW) irradiances in cloud free, single layer and multi-layer clouds. The availability of these different cases in similar synoptic conditions is useful to assess the impact of a cloud layer on an otherwise cloud free atmosphere. Further cloud layers add complexity to such a picture, therefore following the temporal evolution of the ABL with multiple daily profiles, as performed in the second part of the deployment period, proves to be beneficial.
- On cloudy/foggy conditions well-mixed atmospheric boundary layer with constantly low particle concentrations up to the temperature inversion, particle concentrations below 150 nm in size increase aloft on almost every profile, sometime about one order of magnitude.
- In cloudy ABL, the cloud layer influences the LW cooling of the surface, resulting in a net LW irradiance closer to zero. The SW warming of the surface is, in turn, negatively affected by the cloud layer, resulting in smaller SW net irradiances inside and underneath the cloud.
- On sunny days the atmospheric boundary layer is less mixed with increasing concentrations up to the temperature inversion and strongly increasing concentrations of particles below 150 nm in size aloft.
- On sunny days, the LW net flux is negative throughout the entire vertical profile.

- Particle populations of air masses from different source regions differ in terms of particle sizes, with air-masses from S-SE containing one order of magnitude higher concentrations of particles larger than 150 nm.
- On few profiles a strong dynamic in vertical particle distributions, especially in the vicinity of the temperature inversion were observed.

Preliminary results:

- Temperature inversion is a strong barrier that limits the exchange between air masses aloft with the boundary layer.
- It is supposed that small-scale atmospheric dynamics driving changes at the edge of the boundary layer are the major drivers in vertical particle exchange processes.
- Local sources may only contribute to particle concentrations on sunny days when new particle formation can take place.
- Midrange transport is a source of particles with sizes below 150 nm for all wind directions.
- Long-range transport of particles above 150 nm in size from anthropogenic sources is highly depending on prevailing large scale weather conditions and might play a minor role during summer.
- LW cooling is observed inside the cloud, with values up to of -3 K/h in the region of cloud top, decreasing towards cloud base.
- For the observed days, the net irradiance at the surface is positive. Values vary among cloudy and cloud free days.

Data management

All data are handled, documented, archived and published following the MOSAiC data policy (see APPENDIX). A DSHIP action log was created for every balloon profile with the time of profile start/end, operated instruments on the specific profile, maximum altitude and short description of weather conditions during profiling in the comment section.

In the MOSAiC Central Storage (MCS) system the raw data collected during the profiles of each single instrument is saved in the exdata file below the instrument with the according DSHIP entry.

Data will be stored at the PANGAEA data repository (World Data Center PANGAEA), Data Publisher for Earth & Environmental Science www.pangaea.de. DOIs will be communicated to PANGAEA for later access via the future MOSAiC Data Portal.

All data is saved also on different hard drives of Michael Lonardi and Christian Pilz for further handling and distribution to involved PIs without participation in PS122/4.

References

[1] Egerer U, Gottschalk M, Siebert H, Ehrlich A, Wendisch M (2019) The new BELUGA setup for collocated turbulence and radiation measurements using a tethered balloon: first applications in the cloudy Arctic boundary layer. Atmos. Meas. Tech., 12, 4019–4038

3.6 TRACE GAS FLUX & REACTIVE GASES

Byron Blomquist[1,3], Stephen Archer[2]

(not on board): Detlev Helmig[1], Christopher Fairall[3], Laurens Ganzeveld[4], William Sturges[5], Dean Howard[1], Ludovic Bariteau[1,3], Hélène Angot[1], Hans-Werner Jacobi[6], Kevin Posman[2], Sjoerd Barten[4], Lucy Carpenter[8]

[1]EDU.CU
[2]ORG.BIGELOW
[3]GOV.NOAA
[4]NL.WUR
[5]UK.AC.UEA
[6]FR.UGA
[7]UK.AC.YORK

Grant-Nos. NSF OPP 1807496 & NSF OPP 1807163 / NSF OPP 1914781

Objectives

This work encompasses two NSF-funded research projects focusing on air-sea exchange of climate-active trace gases and the atmospheric chemistry of reactive gases, respectively.

Air-sea exchange field work involves eddy correlation (EC) flux measurements of carbon dioxide (CO_2), methane (CH_4), ozone (O_3) and dimethyl sulfide (DMS) from a meteorological tower mounted at the end of the *Polarstern* bow crane. EC flux measurements of CO_2 and CH_4 are also conducted on the sea ice at the MetCity 10m meteorological tower. Additional, discrete flux measurements of CO_2, CH_4 and DMS are done over snow, ice and water surfaces with a dynamic-chamber flux measurement system.

Reactive gases field work is focused on continuous bulk concentration measurements of key reactive species (ozone, nitrogen oxides, volatile organic carbon and halocarbons, and gaseous elemental mercury). These samples are drawn from air inlets on the *Polarstern* bow crane. Additional compressed-flask air samples are collected on a weekly basis for post-cruise analysis of organic carbon and halocarbon species by our collaborators at UEA, and for CO_2/CH_4 by the NOAA GML Greenhouse Gas Monitoring program.

These field measurements form the basis for analysis and modelling of process-level gas transfer mechanisms in the sea ice environment and for modelling reactive trace gas budgets in the atmosphere.

Work at sea

Instrumentation deployed by this project for MOSAiC Leg 4 are listed in Table 3.6.1, including the SensorWeb short name for each device. Except for the flux chambers, flasks and ozone profiler, these are nominally continuous measurements, but there are periods of down-time due to instrument malfunction, maintenance or unsuitable measurement conditions. Figure 3.6.1 shows a timeline for each continuous measurement indicating the periods of operation during Leg 4. Table 3.6.2 lists deployment dates for the dynamic chamber flux system, the species measured, and the surface type sampled. Text in the following paragraphs provides additional detail for each instrument and the measured quantities.

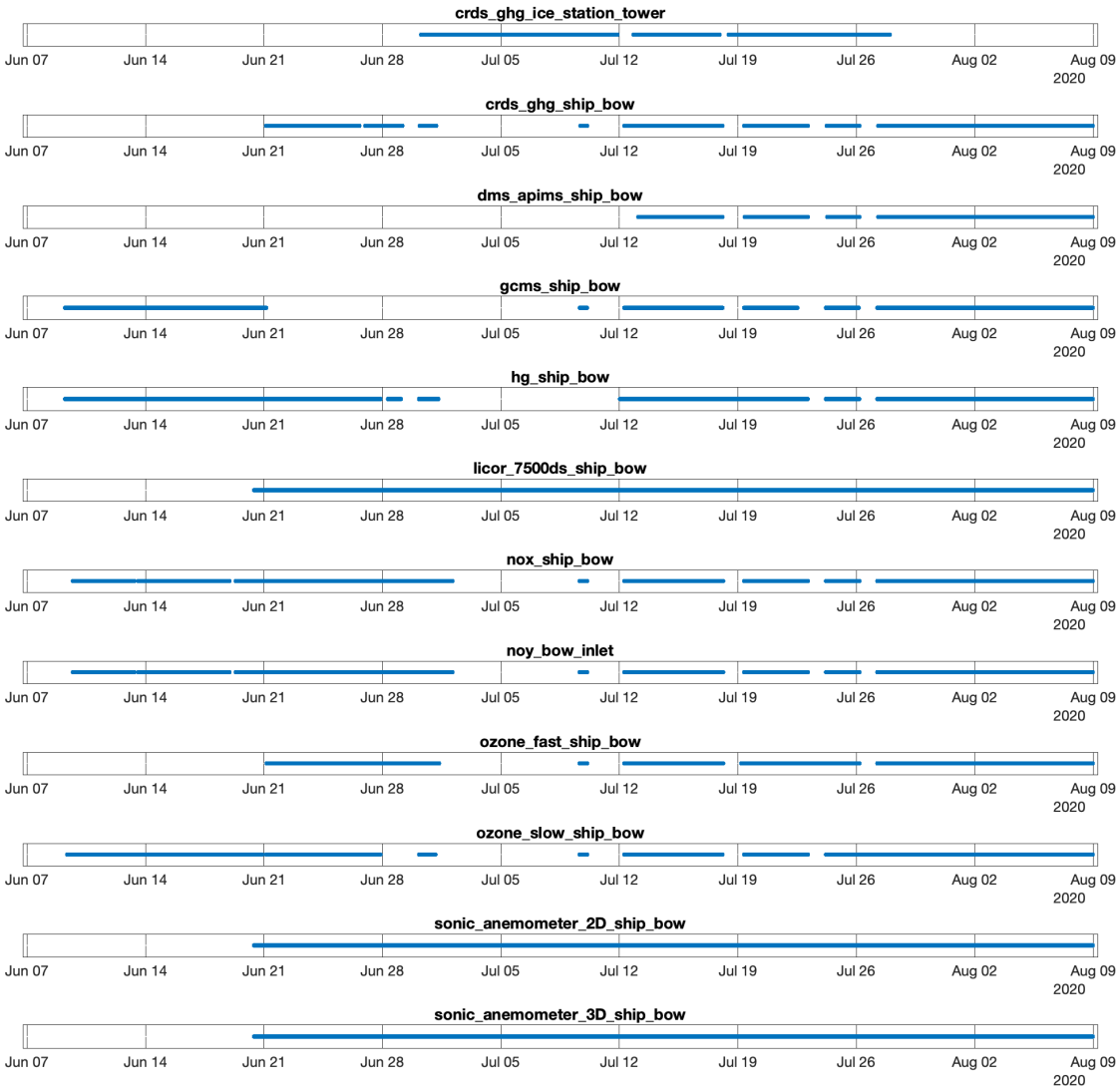

Fig. 3.6.1: Operational timelines for continuous measurement systems deployed during Leg 4.

Tab. 3.6.1: Instruments deployed during Leg 4.

Measurement System	Sampling Location	Sample Rate	SensorWeb 'Short Name'
DMS API Mass Spectrometer	ship bow tower	10 Hz continuous	dms_apims_ship_bow
Picarro G2311-f CRDS	ship bow tower	10 Hz continuous	crds_ghg_ship_bow
Chemiluminescent Ozone	ship bow tower	10 Hz continuous	ozone_fast_ship_bow
Metek uSonic-3 Anemometer	ship bow tower	10 Hz continuous	sonic_anemometer_3D_ship_bow
Licor 7500DS	ship bow tower	10 Hz continuous	licor_7500ds_ship_bow
RM Young 86004 Anemometer	ship bow tower	1 Hz continuous	sonic_anemometer_2D_ship_bow
Chemiluminescent NO/NO2	ship bow crane	10 per minute	nox_ship_bow
NOy inlet for NO/NO2 Analyzer	ship bow crane	10 per minute	noy_bow_inlet
TEI model 49C ozone analyzer	ship bow crane	1 per minute	ozone_slow_ship_bow

Tekran 2537B mercury analyzer	ship bow crane	1 per 5-15 minute	hg_ship_bow
Agilent GC Mass Spectrometer	ship bow crane	~15-18 per day	gcms_ship_bow
Picarro G2311-f CRDS	met city 10m tower	10 Hz continuous	crds_ghg_ice_station_tower
CO2/CH4 Flux Chamber	various	1-3 per deployment	co2_ch4_chamber_portable
DMS Flux Chamber	various	1-3 per deployment	dms_chamber_portable
Ozonesonde Profiler	tethered balloon	1 Hz continuous	ozone_profiler
Geenhouse Gas Flask Sampler	various	~ weekly	gmd_flask_sampler
VOC Flask Sampler	various	~ weekly	uea_flask_sampler

Tab. 3.6.2: Deployments of the dynamic chamber surface flux system during Leg 4.

Deployment Date	**Number of Measurements**			**Gas Species**		
DD/MM/YY	**ice/snow**	**pond**	**lead**	**CO2**	**CH4**	**DMS**
21/06/20	2			X	X	
25/06/20	2			X	X	
28/06/20	4			X	X	
01/07/20		1		X	X	
04/07/20	1	2		X	X	
06/07/20	1	2	1	X	X	X
09/07/20		2	1	X	X	X
11/07/20		2	1	X	X	X
13/7/2020	1	1	1	X	X	X
15/7/2020	1	1	1	X	X	X
18/7/2020			3	X	X	X
19/7/2020		2		X	X	X
21/7/2020		1	2	X	X	X
22/7/2020	2	1		X	X	X
24/7/2020			3	X	X	X
25/7/2020	1	2		X	X	X
26/7/2020	2	2		X	X	X
27/7/2020			3	X	X	X
TOTALS	***17***	***19***	***16***			

The two anemometers (*sonic_anemometer_3D_ship_bow*, *sonic_anemometer_2D_ship_bow*) are standard commercial instruments for wind speed measurement (Metek uSonic-3_Omni, RM Young model 86004), both installed on the bow tower with the 3D sonic at the top of the tower and the 2D sonic about 1.5m lower. The 2D sonic is used for a real-time wind display in the flux laboratory van on E deck. The 3D sonic is used for flux measurements. Gas sampling inlets for CO_2, CH_4, DMS and O_3 flux were located at the base of the 3D anemometer. The bow tower for Legs 1–3 was broken during Leg 3. A shorter replacement tower was installed at the start of Leg 4. The 3D sonic height was ~20m ASL on the original tower and ~18m on the replacement tower. Gas fluxes from the Met City tower are computed with wind data from the University of Colorado 10m sonic operated by the University of Colorado - Shupe project (see Chapter 3.4).

The DMS analyser (*dms_apims_ship_bow*) is a custom-built Atmospheric Pressure Ionization Mass Spectrometer (APIMS) for fast (10Hz) measurement of the DMS concentration (Blomquist et al., 2010). It uses ion-counting to measure the principal ambient DMS isotopomer at mass 63. The ambient DMS concentration is obtained by reference to an isotopically labelled d3-DMS standard at mass 66, continuously added to the sample air stream at the inlet. The DMS concentration is computed using the raw count rates at masses 63 and 66, measured gas flow rates, and the known concentration of the d3-DMS internal standard. This instrument had an electronic failure during Leg 1 and did not operate during Legs 2-3. Following repairs on Leg 4 it resumed measurements on 13 July.

The two Picarro greenhouse gas analysers (*crds_ghg_ship_bow*, *crds_ghg_ice_station_tower*) are commercial cavity-ring-down trace gas analysers specialized for fast, high flow-rate measurement of CO_2 and CH_4 flux (Picarro model G2311-f).

The chemiluminescent fast ozone analyser (*ozone_fast_ship_bow*) is a custom-built system measuring photons emitted by the reaction of ozone with nitrogen monoxide reagent gas (NO) (Bariteau et al.,2010). The ozone concentration is roughly calibrated, and a final calibration will be done post-cruise using reference concentration data from the slow ozone analyser.

The open path Licor (*licor_7500ds_ship_bow*) is a commercial instrument for fast measurement of water vapor and CO_2 (model 7500DS). This was installed on the bow tower, just below the 3D sonic and above the 2D sonic for measuring water vapor flux (latent heat flux). The 7500DS data are only usable when the optics are clean and dry, which was infrequently the case during Leg 4. The CO_2 data from this instrument are not generally reliable for low-level flux measurements due to interferences.

The chemiluminescent NO/NO_2 analyser (*nox_ship_bow*) is a custom-built system operating on the same principle as the fast ozone instrument. In this case, NO concentration is determined from photons emitted by reaction with a high-concentration ozone reagent gas produced by UV irradiation of oxygen. The measurement is calibrated with a compressed NO standard of known concentration. The NO_2 concentration is determined by converting NO_2 to NO with a catalytic converter. The sum of NO and NO_2 is NO_x.

The NO_y inlet (*noy_bow_inlet*) is an addition to the NO/NO_2 analyser which converts other odd-nitrogen species such as nitric acid and peroxyacetylnitrate to NO. This converter is located at the air inlet on the bow crane. The measurement cycle for all the nitrogen species (NO, NO_2, NO_y) is controlled by the data acquisition system on the NO_x analyser. Data files for the NO_y inlet contain flag variables indicating the state of various valves that determine what is being measured at any particular time. Final computation of the concentrations for the various nitrogen species will be done post-cruise.

The slow ozone (*ozone_slow_ship_bow*) and gaseous elemental mercury (*hg_ship_bow*) analysers are both commercial instruments (TEI model 49C and Tekran 2537B).

The Gas Chromatograph – Mass Spectrometer (GCMS) system for volatile organics (*gcms_ship_bow*) is the combination of a custom-built sample collection/standardization

system and a commercial GCMS (Agilent 7820A GC / 5977B MSD). Table 3.6.3 lists the target compounds for this analysis. Calibration is with compressed gas standards from NOAA and UEA. Data analysis requires proprietary software from Agilent and will only be done post-cruise.

Tab. 3.6.3: Target compounds for GCMS measurements during Leg 4.

Hydrocarbons	Halogenated Compounds	Other
Ethane	HFC-125	SF_6
Propane	HFC-134a	OCS
Propyne	HFC-152a	CS_2
Acetaldehyde	HFC-22	Dimethylsulfide
iso-Butane	Methyl Chloride	
n-Butane	CFC-12	
Acetone	HCFC-142b	
iso-Pentane	Methyl Bromide	
Isoprene	HCFC-124	
n-Pentane	H-1211	
Benzene	CFC-114	
Toluene	CH_2Cl_2	
	Methyl Iodide	
	HCFC-141b	
	CFC-11	
	CFC-113	
	chloroform	
	CH_2BrCl	
	CH_2Br_2	
	CCl_4	
	Perchloroethylene	
	$CHBrCL_2$	
	$CHBr_3$	

The dynamic flux chambers (*co2_ch4_chamber_portable*, *dms_chamber_portable*) are custom-built for flux measurements directly on snow, ice or water surfaces with a small footprint (<1m^2) and over short temporal scales of <1hr (e.g., Gao et al, 2011). A constant flow of ambient air is maintained through the chamber volume (8 LPM). Concentrations of CO_2 and CH_4 are measured in the air entering and exiting the chamber using commercial,

portable cavity-enhanced greenhouse gas analysers (Licor models 7810 and 7815). The surface flux estimate is derived from the differential concentration of air entering and exiting, the flow rate through the chamber, and the chamber footprint area. DMS concentrations entering and exiting the chamber are determined by gas chromatography of adsorbent trap samples. The DMS adsorbent trap system operates in parallel to the CO_2/CH_4 analysers. Valves controlling the sampling of inlet and outlet air are programmed with a datalogger (Campbell Scientific model CR6), which also records the chamber flow rate and temperatures.

The ozonesonde profile package (*ozone_profiler*) is a standard ECC ozonesonde modified for use on a tethered balloon to obtain high-resolution boundary-layer O_3 profiles. This was flown on the TROPOS Beluga balloon on two days, 22 and 26 July, recording four profiles (see Chapter 3.5).

In addition to the air measurements, we collected several surface water samples for iodide analysis by a collaborator in the UK (L. Carpenter, York). Surface iodide concentration is an important factor in ozone deposition. Iodide samples are logged, frozen and stored with similar water samples collected for us by the OCEAN, ICE and ECO teams on prior legs. These will be shipped to the UK and analysed post-cruise. Additionally, open lead and melt pond water samples were collected in coordination with chamber flux deployments and analysed for DMS and salinity in our lab van on E deck.

Preliminary (expected) results

Turbulent flux measurements by EC have only been minimally processed, but indications are that most trace gas fluxes are at or below the detection limit. This is partly due to very low fluxes in general and very low windspeeds over the period of Leg 4. Considerable effort will be required post-cruise to QC the data, apply corrections, and estimate detection limits. For flux measurements from the ship there are very few periods when conditions were suitable for turbulence measurements – i.e. when relative wind direction is within a +/- 60° sector of the bow. Figure 3.6.2 is a polar histogram of the 10-minute relative wind direction at the ship's bow for Leg 4. Winds are within the +/- 60° sector about 14% of the time. For the major fraction of the time wind is from the stern of the ship, which contaminates trace gas and flux data on the bow, greatly reducing the amount of usable flux data on this leg.

Wind conditions were more favorable at the Met City tower, but only CO_2 and CH_4 fluxes are measured at this site. The time series of CO_2 and CH_4 concentrations from Met City (Figure 3.6.3), shows these gases are significantly anti-correlated during Leg 4, which is consistent with advection of continental and marine airmasses over our site. Low-CO_2/high-CH_4 events correlate with winds from the E and SE and may indicate spring/summer continental influence, while polar airmasses from the W and N show much less variability in CO_2 and CH_4 concentrations (Figure 3.6.4).

The timeseries of measurements for DMS is shown in Figure 3.6.5. Concentrations were quite low initially. Periods of very high atmospheric DMS concentrations correlate with wind from the SE (Figure 3.6.6). This suggests a very weak local source for DMS and minimal emissions over polar ice to the W and N, with primary source regions over the open ocean and marginal ice zone (MIZ). Concentrations were quite high during recovery activities in the MIZ at the end of Leg 4, where we again had mostly southerly winds.

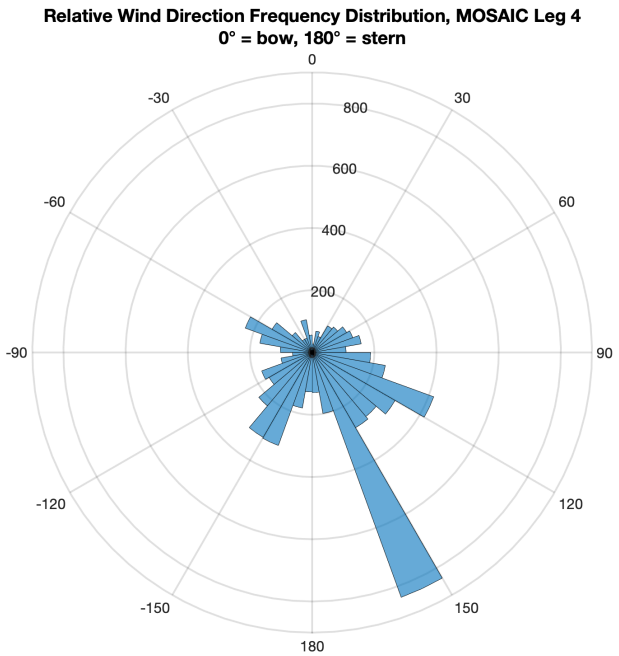

Fig. 3.6.2: Polar frequency distribution histogram for 10-min relative wind direction during Leg 4, as measured by the 2D sonic anemometer on the *Polarstern* bow tower.

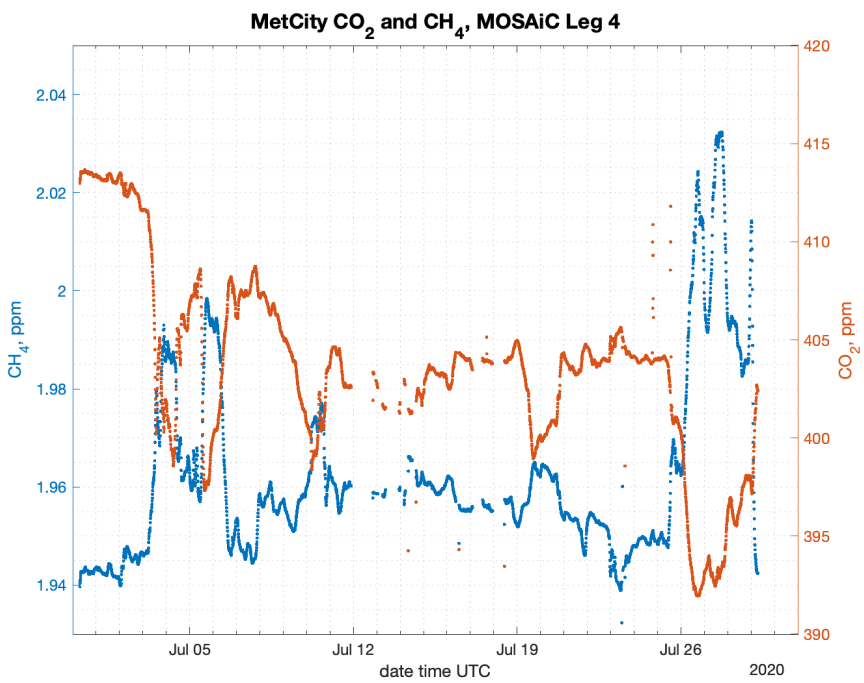

Fig. 3.6.3: Timeseries of CO_2 and CH_4 ambient air concentration at the Met City 10m tower during Leg 4.

Fig. 3.6.4: CO_2 and CH_4 ambient air concentration vs. true wind direction at the MetCity 10m tower during Leg 4.

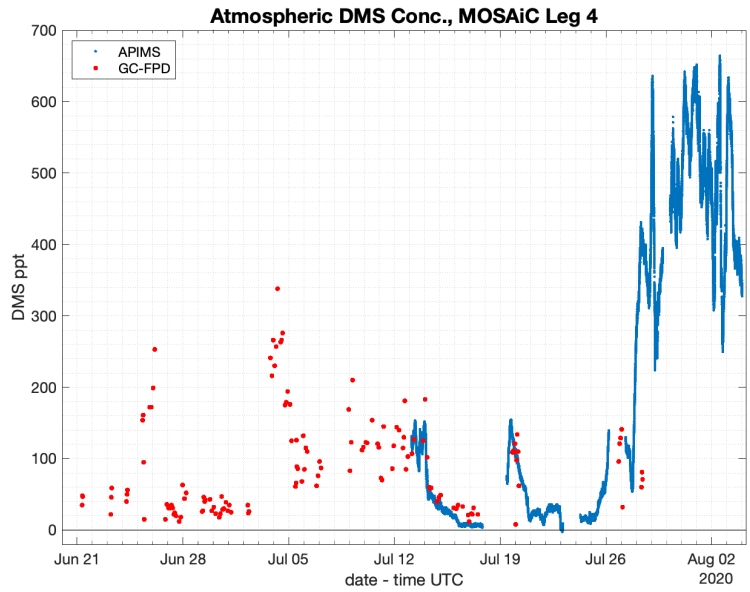

Fig. 3.6.5: DMS ambient air concentration from the ship bow tower during Leg 4. Red markers are discrete air samples collected on adsorbent traps and analysed by GC-FPD. The blue trace is the 10-second mean concentration from the APIMS flux system.

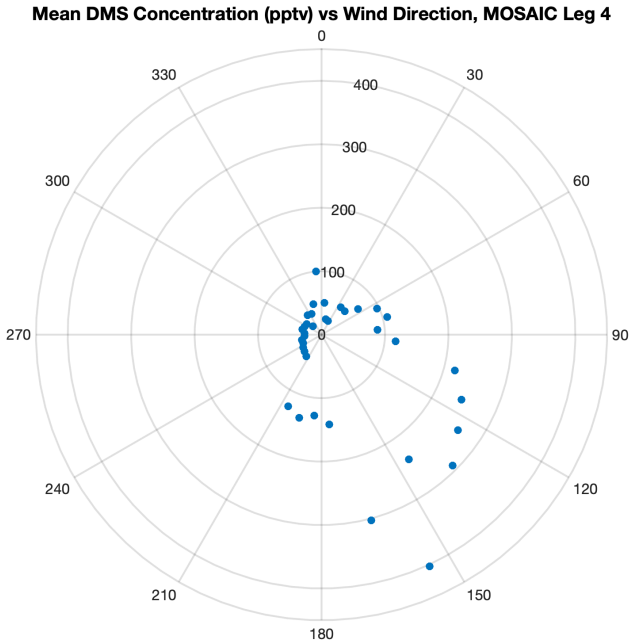

Fig. 3.6.6: Polar plot of DMS air concentration binned by wind direction during Leg 4.

Initial quick looks at reactive gas data (ozone, NOx/NOy, VOCs) are promising. Gas concentration data is usable over a much wider relative wind sector at the bow, up to +/-120°, and this represents about 42% of 10-min periods during Leg 4. Final concentrations for all VOC and NO_x measurements will be processed post-cruise.

Dynamic flux chamber measurements were used to determine exchange of CO_2, CH_4 and DMS over the varied surfaces (Fig. 3.6.7). These measurements aimed to address two specific questions: i) the relative contributions of the different ice/snow, melt pond and open lead surfaces to total CO_2, CH_4 and DMS exchange; and ii) the influence of freshwater input to the ocean surface on trace gas exchange during the melt period. CO_2 and CH_4 exchange rates were measured over 52 individual deployments of the dynamic chamber system over 18 days on both snow/ice and water surfaces. DMS exchange rates were measured during 36 deployments of the combined system. The total amounted to 17 measurements over ice/snow; 19 on melt ponds; and 16 on open leads adjacent to the main floe (Table 3.6.2). Over the majority of deployments, significant flux was detected over the small footprint of the chamber systems, with generally increasing flux of CO_2 and DMS over the course of Leg 4 and consistently low rates of exchange for CH_4. Open lead flux measurements were combined with characterisation of the DMS and salinity profiles across the upper 2 m water column of open leads to investigate the temporal development of the freshwater lens on gas exchange.

Ozone profiles from the Beluga tethered balloon on two days show contrasting characteristics of the atmospheric boundary layer (Figure 3.6.8). On 22 July the boundary layer is reasonably well mixed up to 200 m. On 29 July a strong temperature gradient created stable, stratified conditions near the surface.

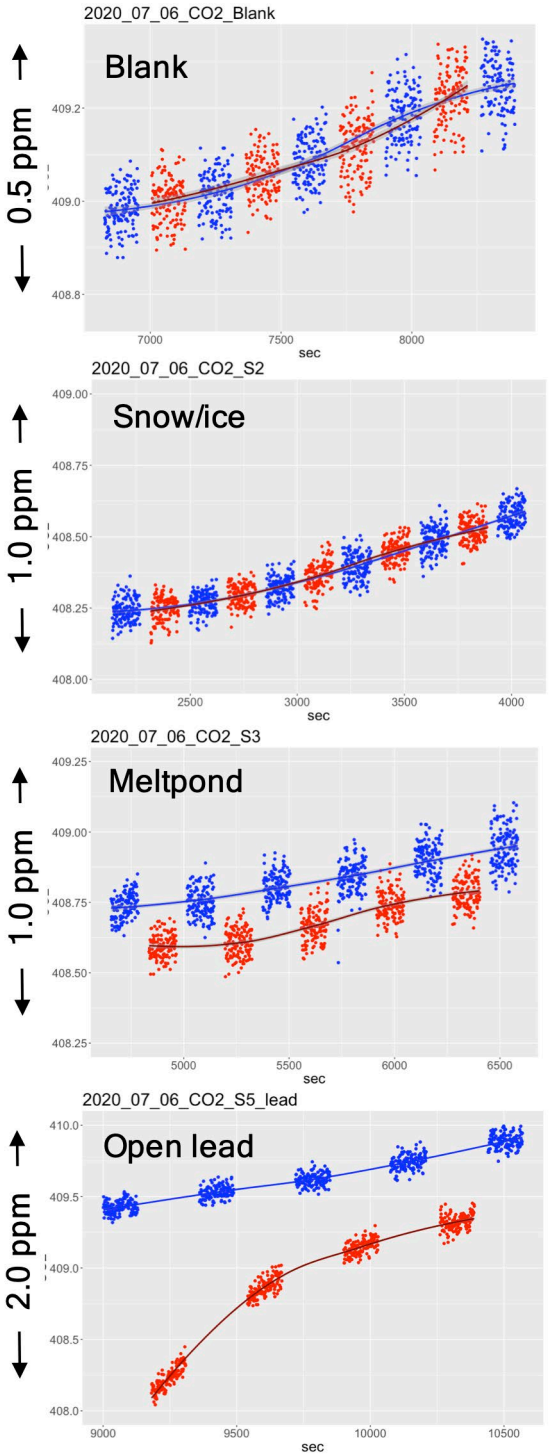

Fig. 3.6.7: Flux chamber records from 6 July 2020 showing CO_2 data from deployment on the different surfaces. The variation in concentrations between ingoing (blue) and outgoing (red) air from the chamber illustrates the extent of the exchange. On this date, minimal exchange occurred across the snow/ice surface, with significant deposition of CO_2 to the melt pond surface and even higher deposition to the open lead.

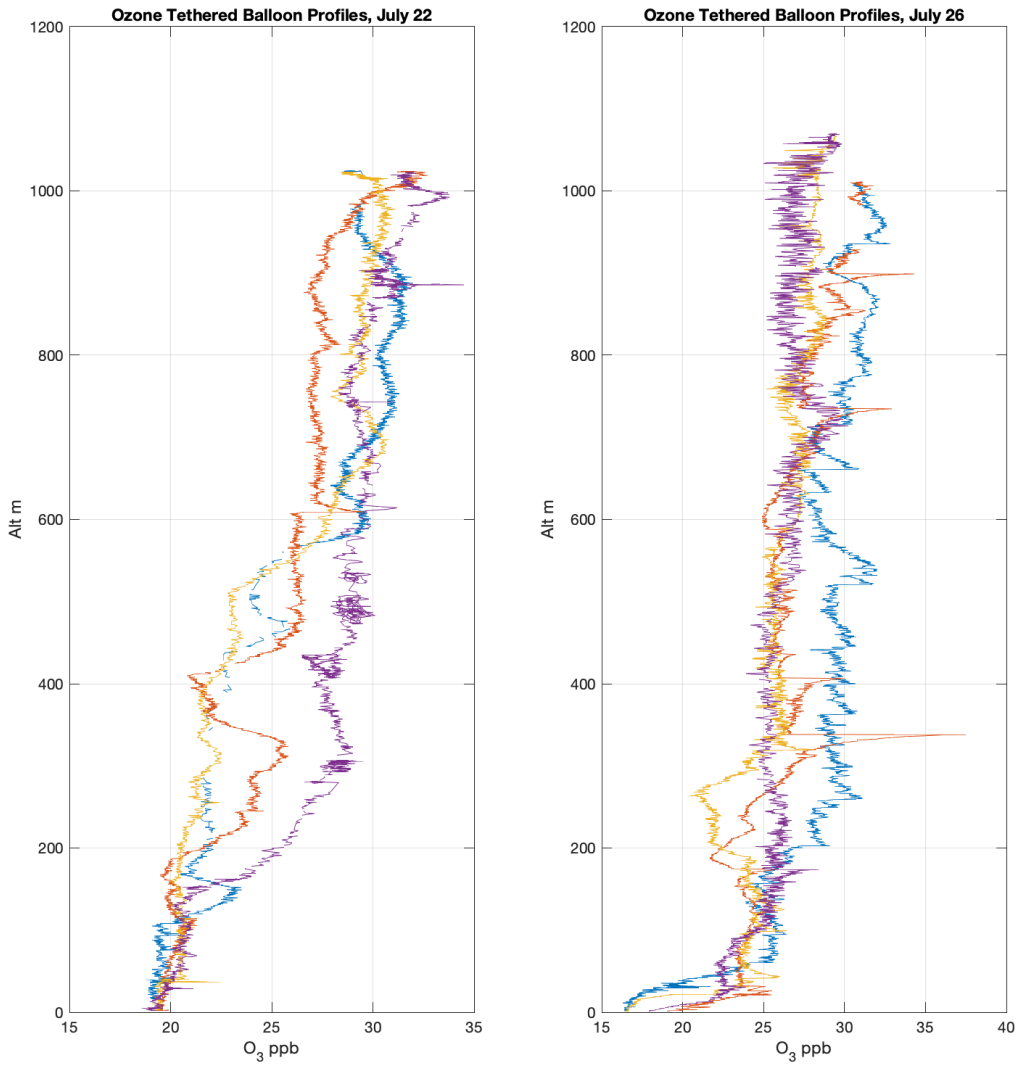

Fig. 3.6.8: Ozone profiles up to 1000m from the TROPOS Beluga tethered balloon during Leg 4.

Data management

All data are handled, documented, archived and published following the MOSAiC data policy (see APPENDIX). Raw data for all sensors has been archived on MCS. Discrete sampling events have been registered in the DShip ActionLog. Some of these discrete samples (air flasks and water samples for iodide) will be analyzed post-cruise and data are not immediately available. We are not directly involved in the analysis of these samples and cannot estimate a completion date at this time.

Data will be stored at the Arctic Data Centre following the agreement between ADC and the MOSAiC Project lead. DOIs will be communicated to PANGAEA for later access via the future MOSAiC Data Portal.

References

Bariteau, L, D Helmig, CW Fairall, JE Hare, J Hueber and EK Lang, (2010), Determination of oceanic ozone deposition by ship-borne eddy covariance flux measurements, *Atmos Meas Tech*, **3**, 441–455, doi:10.5194/amt-3-441-2010

Blomquist, BW, BJ Huebert, CW Fairall, and IC Faloona (2010), Determining the air-sea flux of dimethylsulfide by eddy correlation using mass spectroscopy, *Atmos Meas Tech*, **3**, 1–20, doi:10.5194/amt-3-1-2010

Gao, and others (2011), Chapter 9: Vapor flux measurements–Chamber methods, in: *Vapor Emission to Outdoor Air and Enclosed Spaces for Human Health Risk Assessment: Site Characterization, Monitoring and Modeling,* Nova Science Publishers, Hauppauge, NY, pp. 191-207.

3.7 MEASUREMENT-BASED UNDERSTANDING OF THE NEW PARTICLE FORMATION, AEROSOL BUDGET AND THEIR CLIMATE EFFECTS IN THE ARCTIC

Tuija Jokinen[1]

[1]FI.UNI-Helsinki
[2]CH.EPFL

(not on board:) Ivo Beck[2], Lauriane Quéléver[1], Tiia Laurila[1], Julia Schmale[2], Mikko Sipilä[1], Tuukka Petäjä[1], Markku Kulmala[1]

Objectives

Low-level clouds have an important effect on the surface energy budget in the Arctic. Their lifecycles, warming and cooling effects over the central Arctic Ocean remain unclear, and models fail to correctly simulate them. This shortcoming is partly due to insufficient information on cloud phase (liquid and/or ice crystals). Particularly liquid droplets modulate cloud radiative properties responsible for warming[6]. Droplets form on cloud condensation nuclei (CCN), a subset of aerosol particles. Aerosol particle concentrations over the central Arctic Ocean can be extremely low such that cloud properties are strongly influenced by CCN availability, and in extreme cases cloud formation is even inhibited. Information on aerosol is scarce for all seasons in the high Arctic, but in particular for the cold and dark period when clouds have a pronounced warming effect. To date, only information from land-based stations further south provide proxy information on central Arctic Ocean aerosols in winter.

Our guiding research questions are as follows:

- What are the contributions of natural versus anthropogenic sources to central Arctic Ocean CCN concentrations and how do they vary throughout the seasons (e.g. full sea ice cover in winter vs marginal ice zone in summer)?
- How do new particles form in the Arctic and what is their chemical composition?
- What grows the newly formed particles larger in size?
- Are newly formed particles a source of CCN?
- Which key natural processes are likely to change the CCN budget and control cloud properties with global warming (e.g. diminishing sea ice)?
- How strongly are liquid cloud radiative properties controlled by availability of CCN throughout the seasons?
- What are natural sources of aerosol in general and CCN in particular during the polar night?

With our dataset, we will shed light on the contribution of anthropogenic emissions, other than greenhouse gases, to Arctic warming through cloud formation, characterize for the first time aerosol-cloud interactions during Arctic winter, and help evaluate and improve models for better predictions of Arctic climate change and its far-reaching consequences.

Work at sea

The UHEL-PSI team continued to collect a continuous data set during Leg 4. Our in-situ measurements of aerosol physical and chemical properties, and aerosol precursor and air ion measurements are collected from two containers located on the C-deck on the bow area (position C10, EPFL-PSI container, and C9, BAS container). On top running the PSI-UHEL instrumentation, our task was to deploy Colorado State University's portable aerosol sampler on various locations on the ice and to take care of filter samplers collecting aerosols using

several high and low volume samplers in the British Antarctic Survey's container next door. We also managed some aerosol measurements conducted on the Crow's nest of the vessel.

We operate the instrumentation behind a total inlet (GAW standard) that captures particles and droplets, and an interstitial inlet, which captures only particles that are unable to form cloud droplets. New particle formation events and aerosol precursor gas composition are measured from a specifically designed NPF inlet. The mass spectrometer in the C9 container measures from a simple stainless steel inlet mounted through the roof (APi-ToF inlet). See Figure 3.7.1 for an overview of inlets.

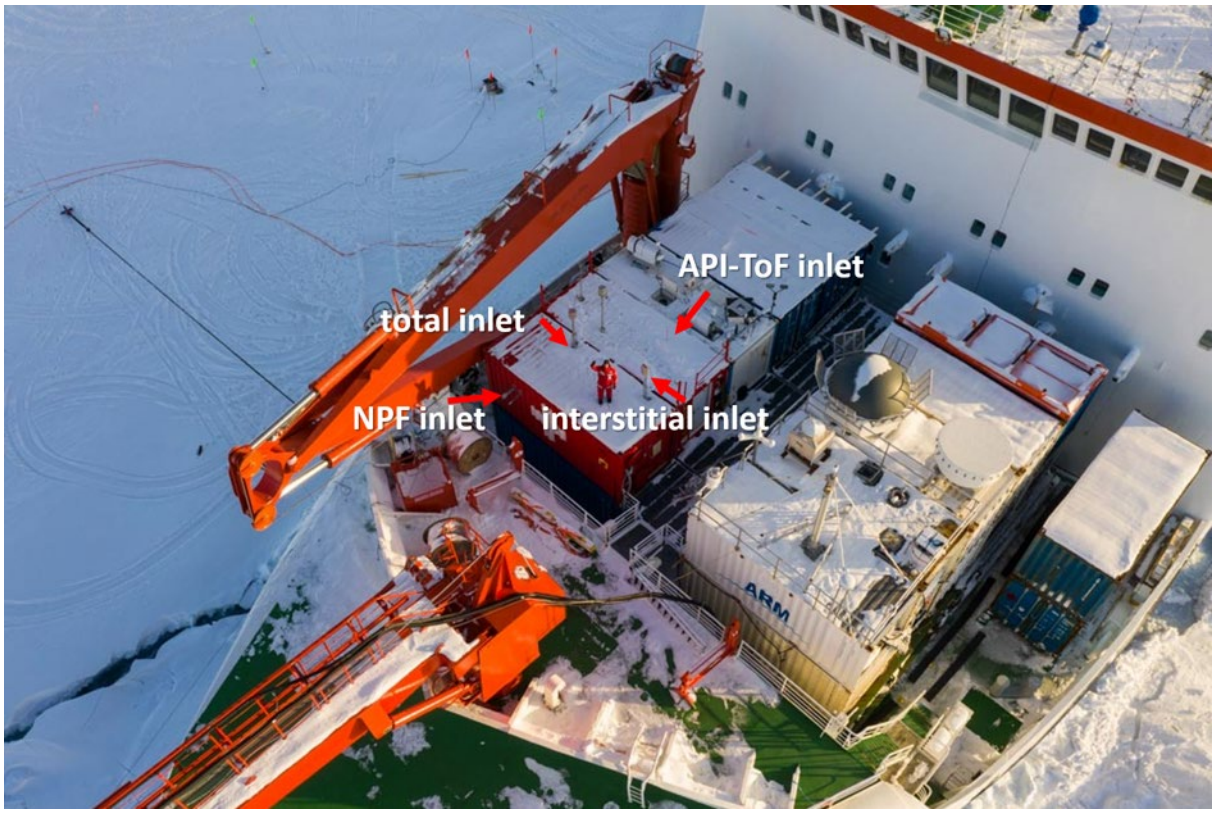

Fig. 3.7.1: Inlets on the EPFL-PSI and BAS containers.

Real-time measurements are carried out by one person during each leg. The main tasks of the operator include ensuring high quality performance of the complex instrumentation set up and maintaining them during the leg. This person's responsibilities also included quality assurance of the measured data set and characterization of natural and anthropogenic events that influenced aerosol formation and population.

With a few exceptions, all instruments operated for the whole period. An overview of all instruments and their working periods is shown in Table 3.7.1. Smaller data gaps that lasted less than one day and are not listed.

Table 3.7.1: Instrumentation and operating periods

ID	Instrument	Location - Inlet	Application	Sampling period
CPC 3776	Condensation particle counter	C10 – Total	Aerosol concentration of the total particle population > 3 nm	8.6.2020 – end of leg 4
CPC 3025	Condensation particle counter	C10 - Interstitial	Aerosol concentration of the interstitial particle population	8.6.2020 – end of leg 4

			> 2.5 nm	
SMPS	Scanning mobility particle counter	C10 – Interstitial & Total	Size spectrum of aerosol population between 14.0746 - 685.39 nm (period 1), and 10.366 – 486.97 nm (period 2)	8.6.2020 – end of leg 4
PSM A11-1 in scanning more	Particle size magnifier	C10 - NPF	Size distribution of the smallest aerosol particles from 1 to 3 nm	8.6.2020 – end of leg 4
PSM A11-2 in step mode	Particle size magnifier	C10 - NPF	Concentration of the smallest aerosol particles. 4 sizes between 1-3 nm.	8.6.2020 – end of leg 4
NAIS	Neutral cluster and air ion spectrometer	C10 – NPF	Size distribution both neutral (2-42 nm) and naturally charged ions (0.8-42 nm). (electrical mobility equivalent diameter)	8.6.2020 – end of leg 4
NAIS stern	Neutral cluster and air ion spectrometer	Stern – top of logistics container	Size distribution both neutral (2-42 nm) and naturally charged ions (0.8-42 nm). (electrical mobility equivalent diameter)	13.7.2020 – 8.8.2020
APS	Aerodynamic particle spectrometer	C10 - Total	Size distribution of the large aerosol population for aerodynamic diameters ranging from 0.5 to 20 µm	8.6.2020 – end of leg 4
CCNC	Cloud condensation nuclei counter	C10 – Interstitial & Total	CCN concentration at supersaturations of 0.15, 0.2, 0.3, 0.5, 1.0 %	Not operational during leg 4.
WIBS	Wideband Integrated Bioaerosol sensor	C10 - Total	Measurement of fluorescently active aerosol for biological speciation between 0.8 and 20 µm	8.6.2020 – end of leg 4
Aethalometer	Aethalometer	C10 – Interstitial & Total	Measurement of equivalent black carbon	8.6.2020 – end of leg 4
AMS	Aerosol mass spectrometer	C10 – Interstitial & Total	Size-resolved chemical composition of submicron aerosol particles (e.g. sulfate, nitrate, organic, ammonium, chloride, …)	8.6.2020 –
CI-APi-TOF	Nitrate-based chemical ionization atmospheric pressure interface time of flight mass spectrometer	C10 - NPF	Aerosol precursor molecule composition measurements. (e.g. Sulfuric acid, Methane sulfonic acid, iodic acid, highly oxygenated organic compounds)	8.6.2020 – end of leg 4
APi-TOF	atmospheric pressure interface time of flight mass spectrometer	C9 – roof inlet	Chemical composition of naturally charged anions and cations, (precursors of aerosols)	Anions: 8.6. – 21.7.2020 30.7.-4.8.2020 8.8.- end of leg 4 Cations: 22.-29.7.2020 & 5.-7.8.2020
O_3	Ozone monitor	C10 - Interstitial	Ozone concentration	8.6.2020 – end of leg 4

SO_2	SO_2 monitor	C10 - Interstitial	Sulfur dioxide concentration	8.6.2020 – end of leg 4
SO_2	SO_2 monitor	C10 - Total	Sulfur dioxide concentration trace levels	8.6.2020 – end of leg 4
Picarro	Picarro Analyzer	C10 - Interstitial	Gas-phase concentration of Methane, Carbon monoxide, Carbon dioxide, water vapor	8.6.2020 – end of leg 4
RH / T 1 & 2	Temperature probe and hygrometer	C10 – Interstitial & Total	Relative Humidity and temperature sensor for both Interstitial and Total inlet	8.6.2020 – end of leg 4
V1	Valve switch	C10 – Interstitial & Total	Hourly bases inlet sample switch for AMS, CCNC, Aethalometer, SMPS	8.6.2020 – end of leg 4
CPC 3022	Condensation Particle counter	C10 - Interstitial	Aerosol concentration of the total particle population > 7 nm	8.6.2020 – end of leg 4
C3PO	Optical particle counter and aerosol filter sampler	Various places across the central observatory	Coarse aerosol size distribution, filter sampling for ice nucleating particle concentrations	12 deployments between 26.6.-28.7.2020
CAPS-CAS	Cloud & Aerosol Spectrometer	Crow's nest	Aerosol size distribution	8.6.2020 – end of led 4
GRIMM-OPC	Optical particle counter	C9 – roof inlet	Aerosol size distribution	8.6.2020 – end of led 4
LoVol	Low volume filter sampler	C9 – roof inlet	INP and halogens – offline analysis	8.6.2020 – end of leg 4
HiVol	High Volume filter sampler	C9 – roof inlet	INP and halogens – offline analysis	One filter weekly
Aerosol filters	Pumps with filter holders	C9-roof	Sugars	Two filters weekly

Expected and preliminary results

The difference between this and the previous legs are that Leg 4 started when *Polarstern* exited the 12 nautical mile zone of Svalbard. For atmospheric research, this was an extremely important and valuable thing to capture how the aerosol population and aerosol precursor gases differ from open ocean and the sea ice edge conditions during summer. The last time this was studied on MOSAiC was when *Polarstern* left Trömsö late last year and freezing of sea ice was the prevailing process, not its melt down.

We did some changes on our measurement set up on the vessel also. We established new neutral cluster and air ions measurements on the stern area due to heavily polluted conditions on the bow during Leg 3 (Figure 3.7.2). This has greatly improved our data coverage of air ions and new particle formation (NPF) event observations. During legs 1-2-3 we only conducted anion measurements with our high-resolution mass spectrometers (CI-APi-TOF and APi-TOF) but during Leg 4, we also collected data on the cation composition for approximately two-weeks.

One of those days were a new particle formation day. Observations of cations (strong bases, ammonia, amines, pyrinides etc.) are so far non-existent from the Arctic and thus highly valuable. We had some setbacks also; unfortunately, during Leg 4 our aerosol mass spectrometer (AMS) suffered a pump failure on 13 July and the spare parts are only delivered with Leg 5 cargo. Our cloud condensation nuclei counter (CCNS) also suffered some fatal electrical issues and we were not able to get any CCN measurements done during Leg 4. Altogether, 20/22 instruments were running 24/7 during Leg 4 and the CSU portable aerosol sampler was deployed 12 times on the ice close to leads and melt ponds.

Fig. 3.7.2: Stern NAIS set up on top of the logistics container.

Overall, conditions for atmospheric measurements were a bit more favourable than during Leg 3. The ship's heading was selected so that the prevailing wind direction would bring clean air to the bow inlets. Unfortunately, the winds did not blow from the forecasted direction (SW) too often. Sulfuric acid data from this leg is partly loss due to contamination from the ship's stack as well as particle number concentration and size distribution data. However, not all aerosol and precursor gas data were affected by exhaust pollution and the data set gives a comprehensive picture of the aerosol processes happening during the Arctic summer with high biological activity in the ocean below.

During Leg 4 we detected a few beautiful NPF events (Figure 3.7.3) we observed during sunny days and those were connected to relatively high concentration of previously known aerosol precursor gases, sulphuric acid, methane sulfonic acid and iodic acid (Figure 3.7.4). We could observe the growth of these particles to over 50 nm when they could act as cloud condensation nuclei. The total number concentration during one strong event rose from clean background conditions (~50 cm^{-3}) up to ~1200 cm^{-3} (Figure 3.7.5).

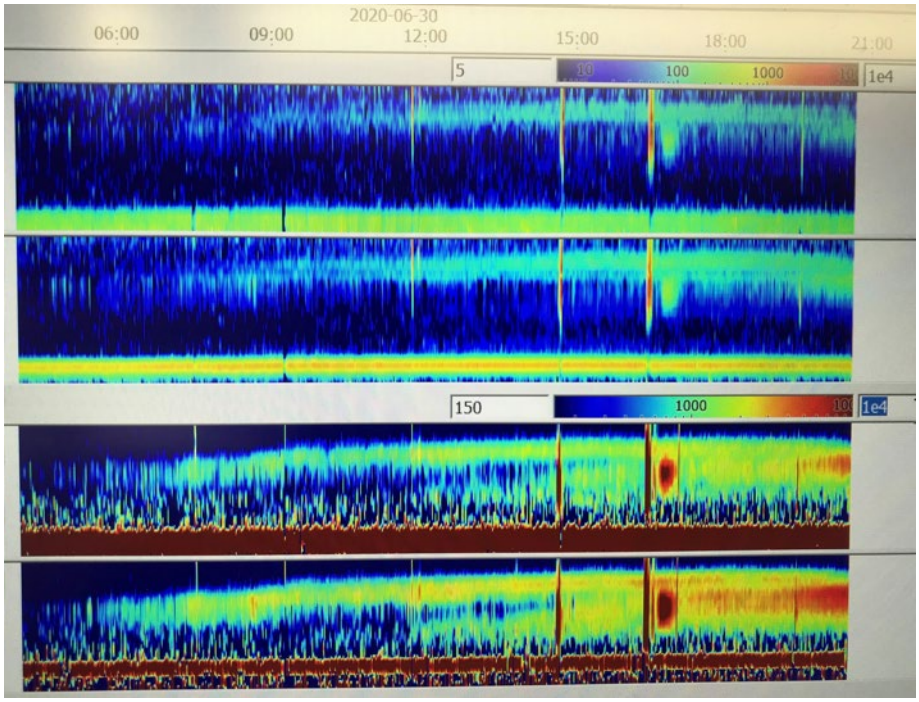

Fig. 3.7.3: Screen shot of the neutral clusters and air ions (measured by a NAIS) during a new particle formation event. The two top panels represent anion and cations concentrations, while the two lower panel represent artificially charged neutral nanoparticles.

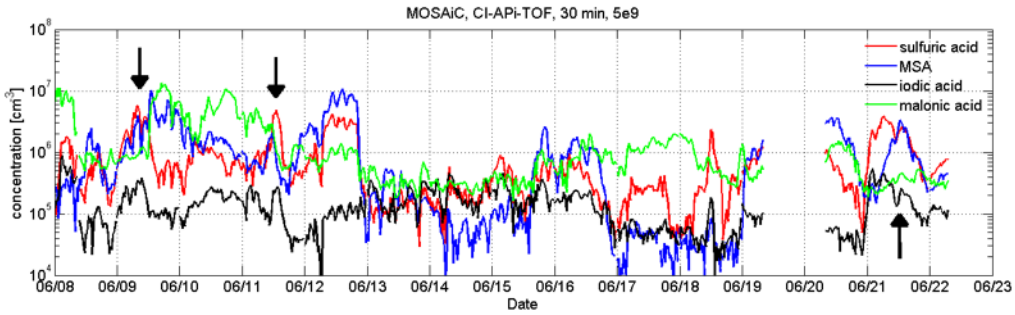

Fig. 3.7.4: Preliminary concentrations of aerosol precursor molecules during the first two weeks of MOSAiC Leg 4. The black arrows show times of NPF and these times have higher concentrations of especially sulphuric acid and methane sulfonic acid (MSA). The data is from the CI-APi-TOF.

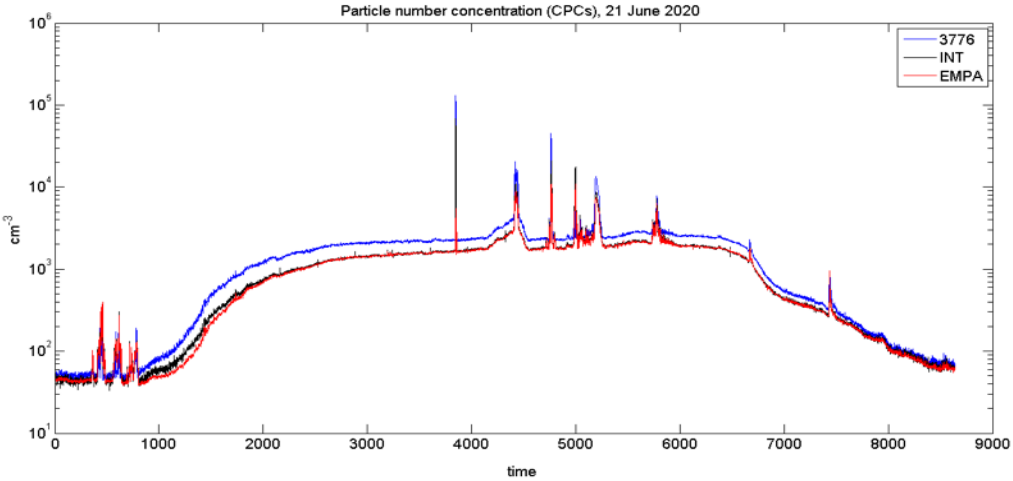

Fig. 3.7.5: Preliminary total number concentration of aerosol particles during one strong NPF day in June. The data is measured with three separate CPCs and they all show comparable results. The spikes in the data are either pollution from the ship or helicopter flights that produce a large number of particles near our sampling site.

If these freshly formed particles actually grew up to CCN sizes, has to be studied further. For this, we will collaborate with ARM aerosol laboratory since our CCN counter was broken during this leg. Also, collaboration with Beluga balloon aerosol measurements with TROPOS is expected to find out the dimensions of NPF, is it happening only at close to ground level or are we observing formation of new particles in the whole boundary layer?

We also collected high quality data of anions during these few NPF event and what we found most interesting was that for the first time, we have possibly detected clusters of sulphuric acid, ammonia and also amines (see Figure 3.7.6). Amines can increase nucleation rates of newly formed particles up to thousand folds in laboratory experiments, but observations from the field are almost completely missing. If these clusters are confirmed in more detailed analysis, the impact is significant. Only two different mechanisms of chemically solving new particle formation starting from the initial clustering exists in the literature that are confirmed in field conditions.

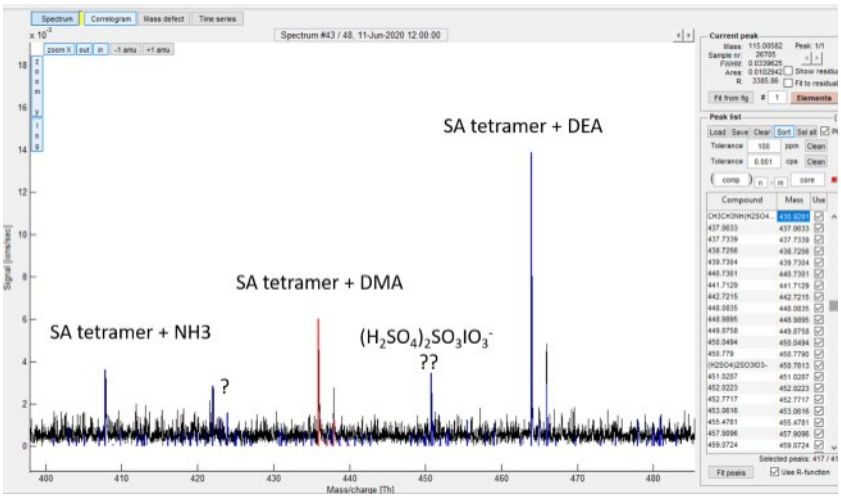

Fig. 3.7.6: Possible/suggested sulphuric acid containing cluster compositions observed during one NPF event day. The data is from the APi-TOF that was set on anion mode measuring naturally charged ion clusters.

One valuable addition to our data set is the seasonal variation of aerosol particles and their precursor gases. MOSAiC campaign has now lasted for more than 300 days and we can observe seasonal trends in our data. For example, in halogen compound concentrations (IO_3, HBr) are below the detection limit of our instrumentation during most of the polar night, but the sun rise starts a series of chemical reactions that produce halogenated compounds in the air. We detected higher concentrations of these compounds during summer but after midsummer they already started to decrease again. It will be intriguing to see what the final long-term data set will look like in the end of leg 5 for these compounds.

Data Management

All data are handled, documented, archived and published following the MOSAiC data policy (see APPENDIX). All instruments are registered in DShip as continuously recording instruments. All raw data are stored on the MCS. Raw data analyses will happen at the institutions involved and intermediate data products will be stored on the servers of the University of Helsinki and École Polytechnique Fédérale the Lausanne. Final data will be stored at the PANGAEA data repository (World Data Center PANGAEA Data Publisher for Earth & Environmental Science www.pangaea.de).

3.9 OBSERVATIONS OF ARCTIC ATMOSPHERIC BOUNDARY LAYER, SURFACE PROPERTIES AND ALBEDO WITH SMALL UNMANNED AERIAL SYSTEMS

Jonathan Hamilton[1], Radiance Calmer[1]

[1]EDU.CU
[2]GOV.NOAA

(not on board:) Gijs de Boer[1,2], Gina Jozef[1], John Cassano[1], Dale Lawrence[1], Brian Argrow[1], Steven Borenstein[1], Abhiram Doddi[1], Michael Rhodes[1]

Objectives

In-situ observations in the high Arctic remain scarce because of difficult access to this remote area and its extreme climate. Consequently, uncertainties associated with the transfer of energy between the surface and the atmosphere is still high for this region. The MOSAiC expedition is the opportunity to gather a substantial data set on atmospheric boundary layer and surface and albedo properties with unmanned aerial systems (UAS). The UAS platforms deployed during Leg 4 of the MOSAiC expedition are designed to provide: 1) detailed information on the vertical structure of lower atmospheric thermodynamic (pressure, temperature, humidity) and dynamic (wind) structure; 2) information on the spatial variability of these quantities, turbulent fluxes of heat and moisture between the surface and atmosphere 3) measurements of surface albedo and surface properties like melt pond fraction and sea ice fraction over the different parts of the MOSAiC floe.

Work on the ice

During Leg 4, three different UAS were deployed on the ice, two fixed-wings – the DataHawk2 and the RAAVEN – and one hexacopter – the HELiX. The characteristics and the associated flight patterns are described in Table 3.9.1 for each platform. The selected payloads to address the scientific objectives (1), (2) and (3) are summarized in Table 3.9.2. The UAS have been flown from two sites on the MOSAiC floe, over the first-year ice, then over the second-year ice, both locations presenting different surface characteristics (thinner ice, open ocean versus thicker ice, sediments embedded in the snow). Additionally, as part of collaborative events with the Ice team, the HELiX flew over the albedo lines and the ROV area for albedo intercomparison. Collocated flight events from the second-year ice site were also organized with the two tethered balloons, the BELUGA from TROPOS and “Miss Piggy” from AWI at several occasions during the Leg 4. Additionally, radiosounding launched three times per day complemented the airborne measurements. The airspace coordination took a large place in the operations to safely share the sky in a restrained area, particularly with the helicopter. At the end of the campaign, as the MOSAiC floe was gone, flights with the HELiX were successfully conducted from the helideck, extending the operation capability of this UAS from the *Polarstern*. To summarize the flight operations with UAS, a total of 91 flights was conducted during Leg 4, for 38.5 hours of airborne time with 34.15 hours of scientific measurements. The DataHawk2 flew 42 flights for 25.78 hours, the HELiX flew 36 flights for 8.68 hours, and the RAAVEN flew 8 flights for only a short airborne time. The RAAVEN data acquisition system demonstrated issues during the expedition; extensive effort and time were dedicated to trouble shoot the problems. Nonetheless, no solution was found with the available resources and a choice was made to concentrate on the operating systems to optimize the time spent on the ice. Three flight tests were also conducted with the UAS from FMI to test the platforms in the Arctic environment. The weather conditions during Leg 4 were mainly low-level clouds, or fog. Few clear sky days occurred during the campaign. However, during these few clear days, many flights were conducted on the same day. 54% of the flights took place in the fog, 14% of the flights were in cloudy conditions, and 32% took place under clear sky.

Tab. 3.9.1: UAS platforms deployed during MOSAiC Leg 4

UAS platforms	DataHawk2	RAAVEN	HELiX
Take-off weight	1.8 kg	4 kg	12 kg
Wingspan	1.1 m	2 m	96 cm
Flight time	45 min	2h15	20 min
Flight patterns	Profile 20-1000 m.asl, Loiter	Profile, loiter, racetrack	Hover, grid
Science objectives	(1) and (2)	(1) and (2)	(3)

Tab. 3.9.2: Payload for each UAS

Instruments	Parameters	Acquisition frequency	Platforms
RSS 421 (Vaisala)	Temperature, relative humidity, pressure	10 Hz	x 1 Datahawk2 x 1 RAAVEN x 2 HELiX
SHT	Temperature, relative humidity	100 Hz	x 1 Datahawk2 x 1 RAAVEN
Cold wire	Temperature	800 Hz	x 1 Datahawk2 x 1 RAAVEN
Hot wire	Turbulence	800 Hz	x 1 Datahawk2 x 1 RAAVEN
IR sensor	Downwelling and upwelling infrared temperatures	100 Hz	x 2 Datahawk2 x 2 RAAVEN
Airspeed, attitude, and ground speed (autopilot)	Wind	10 Hz	x 1 Datahawk2
5-hole probe (BlackSwift), INS (VectorNav)	Wind and turbulence	100 Hz	x 1 RAAVEN
Pyranometers (Kipp and Zonen)	Downwelling and upwelling shortwave radiation	100 Hz	x 2 HELiX
Multispectral camera RedEdge	Pictures of the surface	80 % field overlap	x 1 HELiX

Preliminary (expected) results

Seven profiles from the DataHawk2 flights have been selected to display different weather conditions met during Leg 4, which are summarized in Table 3.9.3. Figure 3.9.1 shows temperature, relative humidity, pressure, potential temperature, and specific humidity from 20 to 1000 m.asl for these seven flights. The conditions during the first flight (blue) were foggy with some icing deposition on the aircraft. A strong inversion was visible at 200 m.asl with an increase of temperature and a decrease of relative humidity. The wind was weak and originated from the North (Figure 3.9.2). The second flight presented hereafter (orange) also took place in foggy conditions, however, the fog was thinner, and some blue sky was sometimes visible above the fog layer. Profiles of temperature and RH presented narrower ranges of values, and the inversion was weaker than the previous flight (blue). The third flight (yellow) took place under a cloud deck at approximately 1000 m.asl, relative humidity was higher than 90% during almost the entire profile, and a weak inversion was visible around 600 m.asl under the cloud. Clear sky days were rare during Leg 4; therefore, numerous profiles were flown the same day, and the fourth flight displayed here (purple) was one of these profiles. A shallow layer is observed over the surface, capped with a strong inversion

around 100 m.asl. The next three flights (green, light blue and red) happened when the wind direction changed from North to East, showing advection of warmer airmasses coming above the floe (Figure 3.9.2). The air temperature above 200 m.asl displayed values higher than 12°C, despite the surface temperature remaining as low as 1°C. These profiles were the last measurements up to 1000 m.asl as thick layers of fog settled down above the floe until the end of Leg 4, preventing any more flights with the DataHawk2.

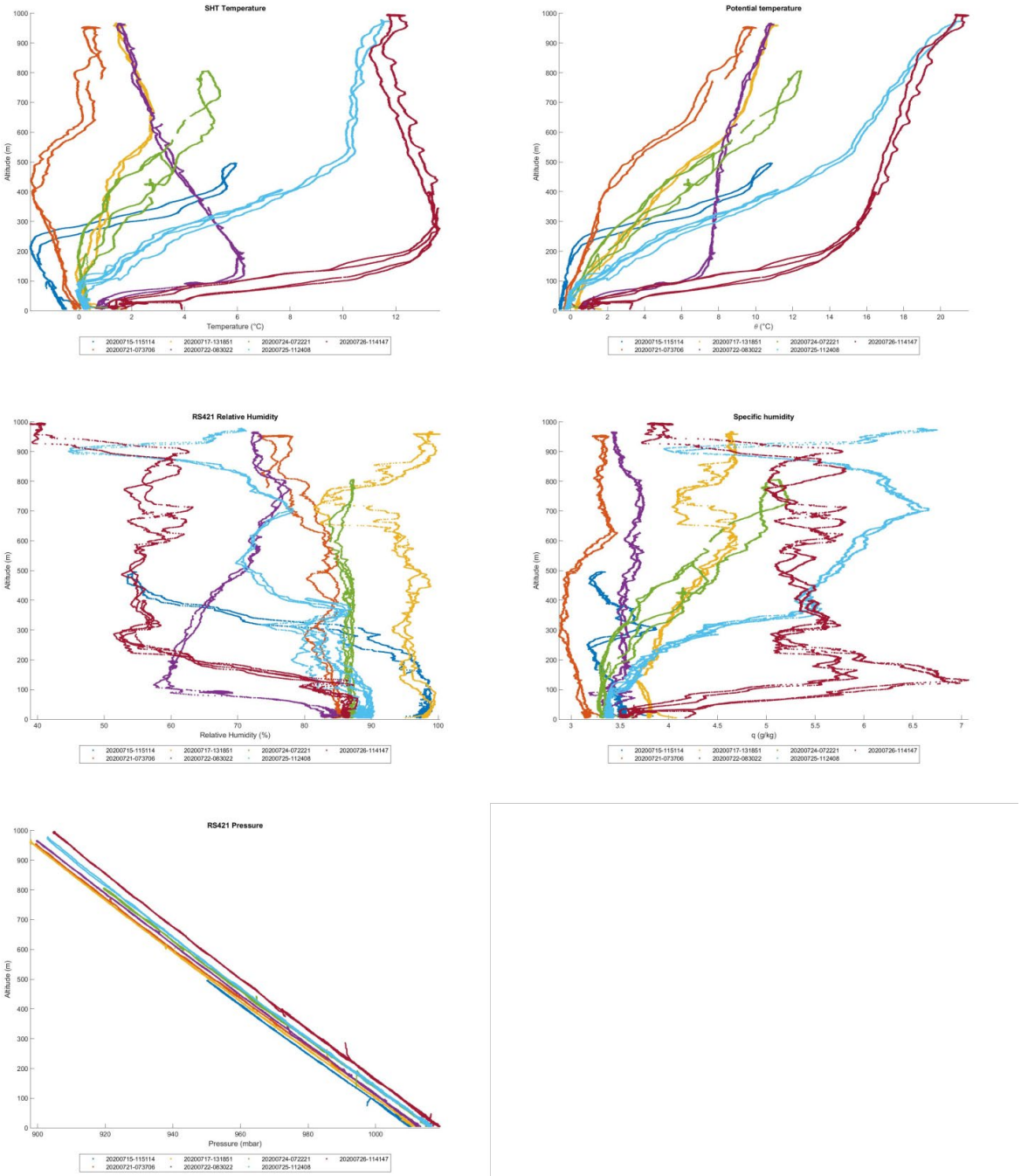

Fig. 3.9.1: Profiles from 20 to 1000 m.asl measured with the DataHawk2 for temperature (SHT sensor), relative humidity (RSS-421 sensor), pressure (RSS-421 sensor), and calculated potential temperature and specific humidity. Seven flights have been selected for different weather conditions summarized in Table 3.9.3.

Tab. 3.9.3: Selected DataHawk2 flights for different weather conditions

Flight date and time	Flight color	Weather conditions
2020/07/15 11:51:14 UTC	Blue	Fog + icing conditions
2020/07/21 07:37:06 UTC	Orange	Fog and pocket of blue sky above
2020/07/17 13:18:51 UTC	Yellow	Cloud deck around 1000 m.asl
2020/07/22 08:30:22 UTC	Purple	Clear sky
2020/07/24 07:22:21 UTC	Green	Warm airmass above inversion
2020/07/25 11:24:08 UTC	Light blue	Warm airmass above inversion
2020/07/26 11:41:47 UTC	Red	Warm airmass above inversion

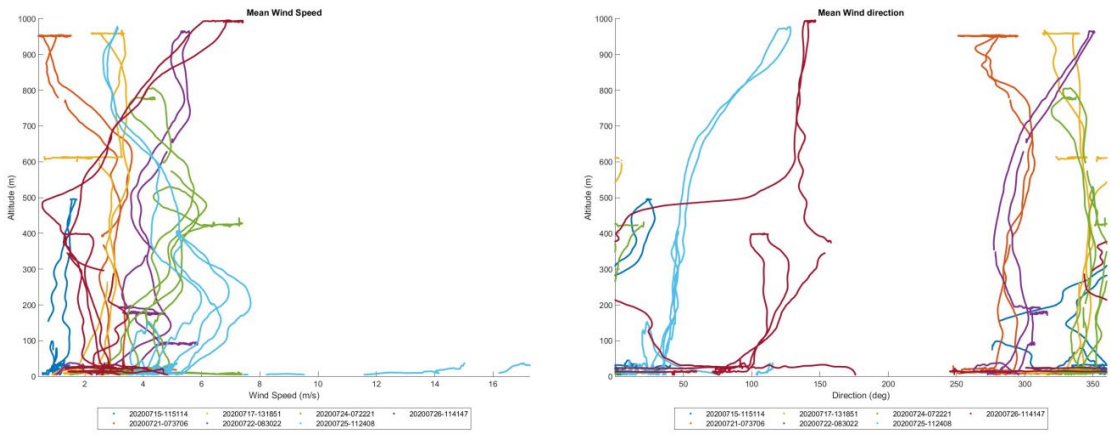

Fig. 3.9.2: Profiles from 20 to 1000 m.asl measured with the DataHawk2 for mean wind speed and direction associated with the seven flights in different weather conditions.

In addition to the atmospheric profiles performed by the DataHawk2, surface properties and shortwave radiation were measured at low altitude by the HELiX. As the MOSAiC floe was formed by first-year and second-year ice, copter flights were conducted above both locations. Figure 3.9.3 presents a grid pattern over the first-year ice area and displays shortwave radiation measured by downward and upward facing pyranometers. Melt pond, ridges, patches of snow, and open ocean were overflown at 10 m.asl by the HELiX. The presence of the open ocean on the left part of the grid pattern is significant in the downward facing pyranometer measurements (<40 W/m² compared to >100 W/m² above the sea ice). The sky was cloudy during this flight with a ceiling lower than 500 m.asl. The presence of mid-level clouds is seen in the uniform shortwave radiation (~250 W/m²) measured by the upward facing pyranometer. Figure 3.9.4 introduces measurements of shortwave radiation over the second-year ice. Values of the downward facing pyranometer present more progressive spatial variations as the floe is mainly covered by melt ponds and patches of snow. However, the upward facing pyranometer captured the transition between thinner fog with visible blue sky above and thicker fog, progressively reducing the visibility, with values peaking at 250 W/m² (first grid pattern), then decreasing to 170 W/m² (second grid pattern). Figure 3.9.5 shows an example of pictures in five different channels taken by the multispectral camera over a melt pond. The structure of the sea ice under the fresh water is clearly visible. Analysis of the pictures from the HELiX flights will reveal more information about the different fractions of the floe (snow, melt pond, ridge), and complement observations of shortwave radiation to understand the contribution of each feature to the albedo.

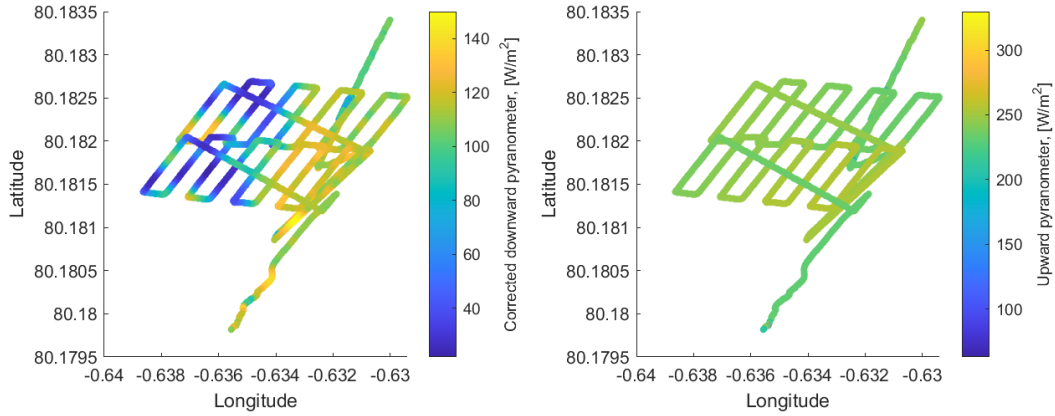

Fig. 3.9.3: Grid pattern with the HELiX UAS at 10 m.asl over the first-year ice part of the MOSAiC floe. Shortwave radiation measured by downward and upward facing pyranometers.

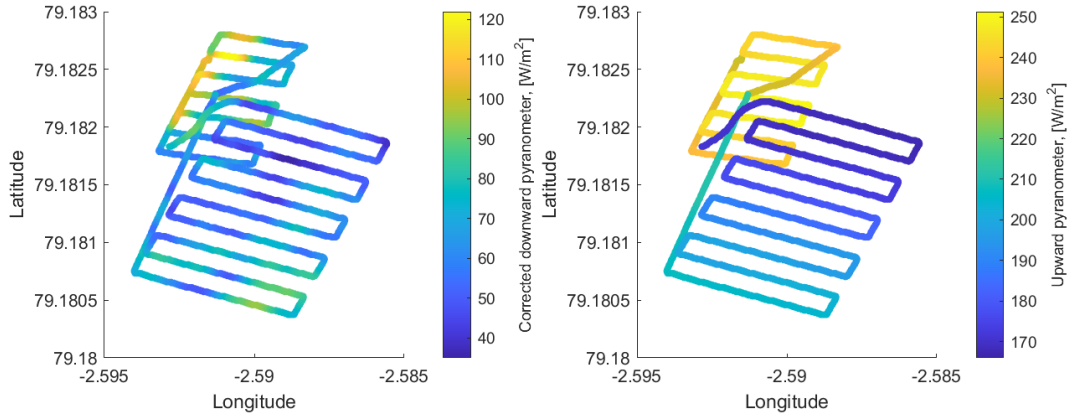

Fig. 3.9.4: Grid pattern with the HELiX UAS at 10 m.asl over the second-year ice part of the MOSAiC floe. Shortwave radiation measured by downward and upward facing pyranometers.

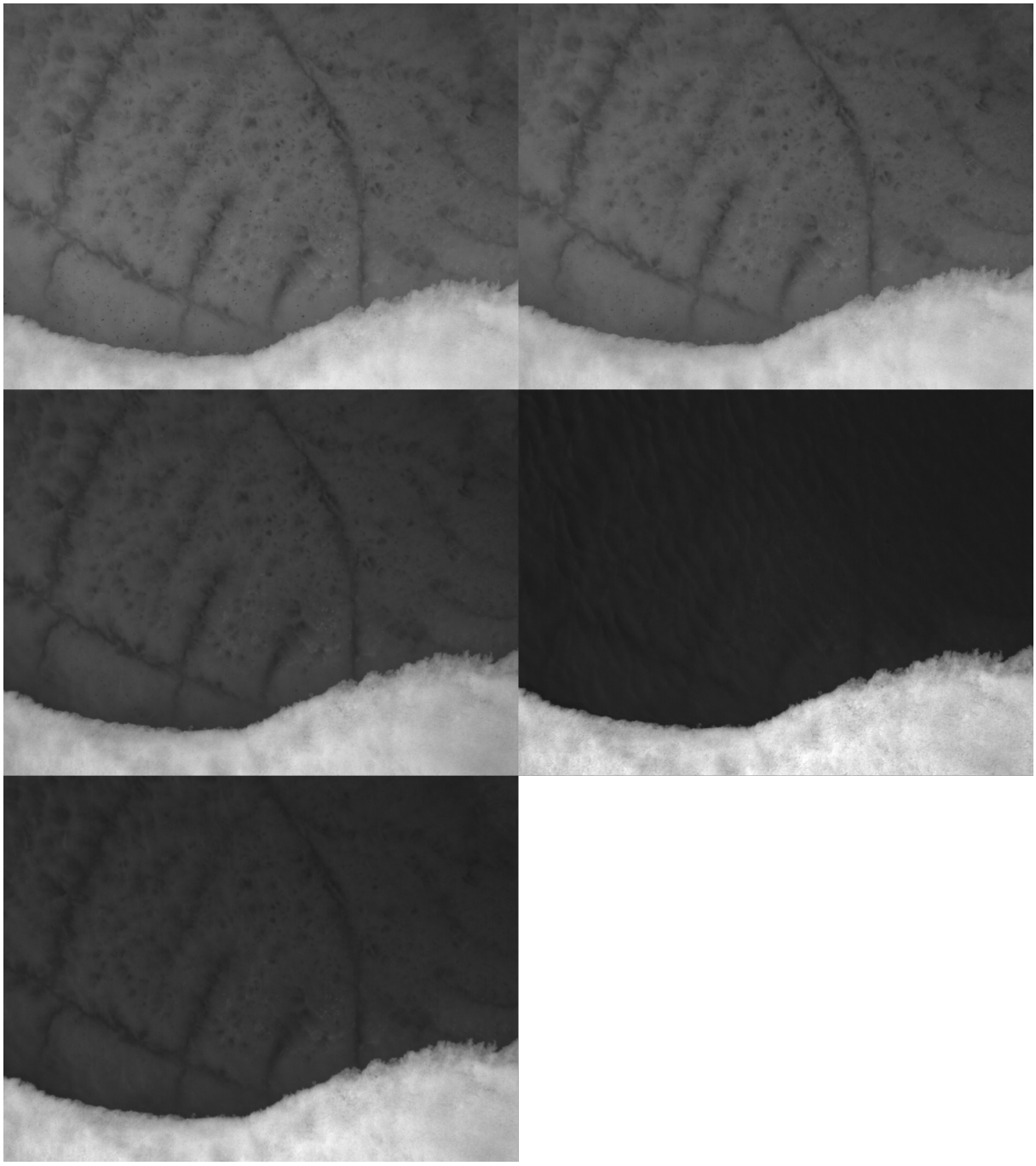

Fig. 3.9.5: One picture from different channels of the multispectral camera over a melt pond during a HELiX flight.

Data management

All data are handled, documented, archived and published following the MOSAiC data policy (see APPENDIX). Preliminary processed B1 datafiles and quicklooks are available on the MCS for the DataHawk2 flights. The device operation for the HELiX and RAAVEN flights have been created on DSHIP. Processed data from the HELiX flights will be uploaded on SENSORWeb later. Final data will be stored at the Arctic Data Centre following additional quality control in accordance with the agreement between ADC and the MOSAiC Project lead. DOIs will be communicated to PANGAEA for later access via the future MOSAiC Data Portal. All data are handled, documented, archived and published following the MOSAiC data

policy. It is expected that data papers will be prepared and submitted to Earth System Science Data documenting these datasets.